ISTANBUL TECHNICAL UNIVERSITY ★ GRADUATE SCHOOL OF SCIENCE ENGINEERING AND TECHNOLOGY

SYNTHESIS AND CHARACTERIZATION OF STRONTIUM ALUMINATE BASED NANOPHOSPORS

M.Sc. THESIS

Mehmet Durmuş ÇALIŞIR

Department of Nano-Science and Nano-Engineering

Nano-Science and Nano-Engineering Programme

Thesis Advisor: Asst. Prof. Dr. Nuri SOLAK

AUGUST 2014

ISTANBUL TECHNICAL UNIVERSITY ★ GRADUATE SCHOOL OF SCIENCE ENGINEERING AND TECHNOLOGY

SYNTHESIS AND CHARACTERIZATION OF STRONTIUM ALUMINATE BASED NANOPHOSPORS

M.Sc. THESIS

Mehmet Durmuş ÇALIŞIR

513121013

Department of Nano-Science and Nano-Engineering

Nano-Science and Nano-Engineering Programme

Thesis Advisor: Asst. Prof. Dr. Nuri SOLAK

Department of Metallurgical and Materials Engineering

AUGUST 2014

İSTANBUL TEKNİK ÜNİVERSİTESİ ★ FEN BİLİMLERİ ENSTİTÜSÜ

NANO BOYUTTA STRONSİYUM ALUMİNAT ESASLI FOSFOR SENTEZİ VE KARAKTERİZASYONU

YÜKSEK LİSANS TEZİ

Mehmet Durmuş ÇALIŞIR

513121013

Nano-Bilim ve Nano-Mühendislik Ana Bilim Dalı

Nano-Bilim ve Nano-Mühendislik Programı

Tez Danışmanı: Yrd. Doç. Dr. Nuri SOLAK

Metalürji ve Malzeme Mühendisliği Bölümü

AĞUSTOS 2014

Mehmet Durmuş ÇALIŞIR, a M.Sc. student of ITU Graduate School of Science Engineering and Technology student ID 513121013, successfully defended the thesis entitled "SYNTHESIS AND CHARACTERIZATION OF STRONTIUM ALUMINATE BASED NANOPHOSPORS", which he prepared after fulfilling the requirements specified in the

Thesis Advisor: **Asst. Prof. Dr. Nuri SOLAK**
Istanbul Technical University

Jury Members: **Prof. Dr. Mustafa Kamil ÜRGEN**
Istanbul Technical University

Assoc. Prof. Dr. Esra ALVEROĞLU
Istanbul Technical University

Date of Submission : 04 August 2014

Date of Defense : 08 August 2014

To my wife, family and friends

FOREWORD

I would like to express my gratitude to my thesis supervisor, Asst. Prof. Dr. Nuri SOLAK, for his continuous encouragement and guidance during my graduate studies and for his helpful critiques and discussions on my work.

I would like to thank Assoc. Prof. Dr. Esra ALVEROĞLU for her support and guidance.

I especially would like to thank my friends in the ITU laboratory: Ersu LÖKÇÜ, Rıfat YILMAZ and Ahmet YAYLA for their collaboration and friendship.

I would also like to extend my deepest gratitude to my wife S. Şeyma ÇALIŞIR, to my elder brother M. Fatih ÇALIŞIR and to my family. For all those times they stood by me and heartedly supported. I was able to accomplish everything in my life thanks to their eternal love.

Finally, I would like to thank all of my friends for their emotional support and motivation during this difficult accomplishment.

August 2014

Mehmet Durmuş ÇALIŞIR

Metallurgical and Materials

Engineer

TABLE OF CONTENT

Page

ABBREVIATIONS

SEM **:** Scanning Electron Microscopy

XRD **:** X-Ray Diffractometer

PL **:** Photoluminescence

UV **:** Ultraviolet

LED **:** Light Emitting Diode

RA **:** Reductive Atmosphere

LIST OF TABLES

Page

LIST OF FIGURES

Page

SYNTHESIS AND CHARACTERIZATION OF STRONTIUM ALUMINATE BASED NANOPHOSPORS

SUMMARY

Persisting light emission from a substance after the exciting radiation has removed is known as phosphorescence. Phosphorescence occurs when appropriate elements with suitable electronic configuration are doped into certain host materials. Both the dopant ions and the host material have critical importance to achieve efficient phosphorescence emission (long after glow time and high intensity). Strontium aluminate co-doped europium and dysprosium ($SrAl_2O_4:Eu^{2+}$, Dy^{3+}) is one of the known green light emitting persistent phosphorescent materials. $SrAl_2O_4:Eu^{2+},Dy^{3+}$ phosphors have been used in several application areas such as emergency signs used in airports and highways, paints, ceramic products, accessorizes, LEDs and plasma display panels due to their high initial luminescent intensity, long lasting time, suitable emitting color and good chemical and thermal stability. This long afterglow effect has been ascribed to the recombination of the trapped $SrAl_2O_4:Eu^{2+},Dy^{3+}$ electrons at europium(II) sites and the thermally released holes trapped at dysprosium(III) sites.

The present study aims to synthesize $SrAl_2O_4:Eu^{2+},Dy^{3+}$ phosphor with solid state, sol-gel and solution-combustion methods and investigate the effects of nano size on the phosphorescence characteristics. Therefore, we also investigate the effect of co-doping with Fe, Ni, Co and Y on the phosphorescence properties. In experimental study, different samples were prepared according to formula $Sr_{0,92-x}M_XAl_2O_4:Eu_{0,02}Dy_{0,06}$ (M: Fe, Ni, Co and Y) where x is 0.005 and 0.01 in molar ratio with addition % wt 2.5 boric acid as a flux material. All samples synthesized with solid state and both of sol-gel and sol-combustion methods were sintered at 1300C in %5 H_2-N_2 reductive atmosphere to reduce Eu^{3+} to Eu^{2+} whose emission is correspond to 515 nm wavelength due to 4f-5d electronic transitions. XRD, SEM and spectrophotometer were used to investigate the structural, morphological and optical analysis, respectively. It is observed that the monoclinic $SrAl_2O_4$ is the main phase in the XRD patterns of all samples. According to SEM micrographs, all samples have highly sintered microstructure. Emission at about 510 nm and excitation by wide wavelength range (generally 300-450 nm) was observed from UV-Visible Spectrophotometric analysis.

NANO BOYUTTA STRONSİYUM ALUMİNAT ESASLI FOSFOR SENTEZİ VE KARAKTERİZASYONU

ÖZET

Maddelerin akkor ısı kaynaklarından farklı olarak ısısı değişmeksizin ışık yayması olayına lüminesans denir. Bir başka deyişle lüminesans, temel halden uyarılmış hale geçen elektronların tekrar temel hale geçişleri esnasında foton yayınımı yapmasıdır. Uyarma kaynağının türüne bağlı olarak fotolüminesans çeşitli başlıklar altına gruplanır. Eğer lüminesans maddelerin uyarılması ışığın emilimi ile olup, bunun sonucunda görünebilir bölgede ışıma elde ediliyorsa bu durum fotolüminesans olarak adlandırılır. Uyarılmış durumların yapısına bağlı olarak organik malzemelerde fotolüminesans ikiye ayrılarak incelenir. Bunlardan birincisi floresans ve diğeri ise fosforesanstır. Floresans olayında elektronlar singlet uyarılmış seviyedir. Bu durumda elektron spini uyarılmış seviyede de korunmuştur. Uyarılmış seviyedeki ve temel durumdaki elektronlar bir çift oluştururlar ve temel seviyeye geçiş yine singlet halde gerçekleşir. Uyarılmış halden temel seviyelere geçiş çok hızlı gerçekleşir. Dolayısıyla ışık kaynağının uzaklaştırılmasının ardından floresan malzemeler ışıldamasını çok hızlı kaybeder. Fosforesans durumunda uyarılmış elektronlar spin yönlerini değiştirerek triplet uyarılmış halde bulunurlar. Triplet uyarılmış seviyeden temel seviyeye dönüşte bu elektronların spinleri tekrar değişir ve bu durum zaman gerektirir. Dolayısıyla ışık kaynağının uzaklaştırılmasının ardından fosforesan malzemeler ışıldamasını yavaş bir şekilde kaybeder. Eğer maddenin ışıldaması yeterince uzun sürüyorsa bu tür maddeler karanlıkta parıldayan maddeler olarak adlandırılır.

İnorganik malzemelerde ise fosforesans ışık kaynağının kaldırılmasından sonra insan gözüyle algılanabilir şekilde uzun süreli ışıldama olayıdır. İnorganik fosforesan malzemelerde bu durum kuantum mekaniğinde yasaklanmış enerji seviyeleri arasındaki geçişler ile ilişkilendirilir. Fosforesans uygun elektronik konfigürasyona sahip elementler ile katkılandırılmış belirli matris malzemelerde görülmektedir. Etkin bir fosforesans yayınımı için (uzun süreli ışıma ve yüksek ışıma şiddeti) katkı elementleri ve matris malzemeler çok kritik öneme sahiptir. Evropiyum ve disprozyum elementleri ile katkılandırılmış stronsiyum aluminat ($SrAl_2O_4:Eu^{2+}$, Dy^{3+}) fosforlar uzun sureli ışıma yapan fosforlardan biri olarak bilinmektedir. Bu fosforlar yüksek ışıma şiddeti, uzun ışıma süresi, uygun ışıma rengi ve kimyasal ve termal kararlığı özelliklerinden dolayı havalimanları ve otoyollarda acil durum işaretlerinde, boyalarda, seramik ürünlerde, aksesuarlarda, LED'lerde ve plazma görüntü panellerinde kullanılmaktadır.

$SrAl_2O_4:Eu^{2+}$, Dy^{3+}temelli fosforlarda fosforesans, Eu^{+2}'nin 4f → 5d elektronik geçişlerinden kaynaklanmaktadır. Bu fosforlarda $SrAl_2O_4$ etkin bir matris malzeme görevi görürken evropiyum lüminesans merkezi ve disprozyum da tuzaklama

merkezi olarak görev yapar. $SrAl_2O_4:Eu^{2+}$, Dy^{3+} fazının uzun süreli ışıma özelliği evropiyum(II)'nin 5d elektron seviyelerinin iletim bandına çok yakın olması, uyarılan elektronların iletim bandına kolayca geçip, disprozyum(III) bölgelerinde tuzaklanması ile açıklanmaktadır. Tuzaklanan bu elektronlar termal olarak yavaşça serbest kalıp, tekrar temel hallerine dönerken uzun süreli ışımaya neden olmaktadır.

Yapı içerisindeki Eu^{+2}'nin 4f elektronları, en dış kabuğun kalkan görevi görmesi dolayısıyla, yapıdaki değişikliklere karşı güçlü olmasına rağmen, 5d elektronları bu değişimlerden kolayca etkilenebilir. Dolayısıyla Eu^{2+}farklı kristal yapılarında farklı dalga boylarında ışıma göstermektedir. Örneğin Eu^{2+} ve Dy^{3+} katkılı $SrAl_2O_4$yeşil ışık yayarken, aynı elementler ile katkılandırılmış $Sr_2MgSi_2O_7$ mavi ışık yaymaktadır. Eu^{+2}'nin 5d seviyeleri aynı kristal yapı içerisinde tane boyutu değişimi ve farklı element türlerinden de kolayca etkilenmektedir. Eu^{2+},Dy^{3+} katkılı $SrAl_2O_4$ 520 mm'ye karşılık gelen yeşil ışıkta ışıma yaparken, aynı katkılar yapılmış $BaAl_2O_4$ 500 mm'de ışıma yapması; $SrAl_2O_4$'ın tane boyutu mikrometre mertebelerinden nanometre seviyelerine azalırken yayınım renginin yeşilden maviye kayması bu durumlara birer örnektir.

Bu çalışmada $SrAl_2O_4:Eu^{2+}$, Dy^{3+} fosforunun mikro ve nano boyutta geleneksel seramik, sol-gel ve solüsyon-yanma yöntemleri ile sentezlemek ve nano boyutun fosforesans karakterine etkileri araştırmak amaçlanmıştır. Ayrıca geçiş metallerinden demir (Fe), nikel (Ni), kobalt (Co) ve nadir toprak elementlerinden itriyum (Y)'un fosforesans özelliklerine etkisi de incelenmiştir. Deneysel çalışmalarda, $Sr_{0,92-x}M_XAl_2O_4:Eu_{0,02}Dy_{0,06}$ (M: Fe, Ni, Co ve Y; X=0.005 ve 0.01) birleşiminde ağırlıkça % 2,5 borik asit katkılı numuneler sentezlenmiştir. Elde edilen bütün numuneler 1300°C de %5 H_2-N_2 indirgeyici atmosferde ısıl işleme tutulmuş ve Eu^{3+}'ün Eu^{2+}'ye indirgenmesi sağlanmıştır. Elde edilen numunelerin yapısal, morfolojik ve optik analizleri XRD, SEM ve spektrofotometre cihazları ile gerçekleştirilmiştir.

Katı hal yöntemiyle sentezlenen fosforların ağırlıkla monoklinik $SrAl_2O_4$ fazında olduğu ve nano mertebede tane boyutlarına sahip numuneler elde edildiği anlaşılmıştır. Reaksiyon süresinin artmasıyla hem XRD piklerinin hem de spektrofotometrik analiz eğrilerinin şiddetlerinin artığı gözlemlenmiştir. Sol-jel ve yanma reaksiyonu ile üretilen numunelerin ise sadece monoklinik $SrAl_2O_4$ fazı içerdiği gözlemlenmiştir. Bu yöntemler katı hal yöntemine göre daha hızlı ve daha saf ürün verdiği deneysel sonuçlarla doğrulanmıştır. SEM mikrograflarına bakıldığında yapının yüksek derecede sinterlenmiş bir morfolojide olduğu gözlemlenmiştir.

Optik analiz sonuçlarına göre bütün numuneleri 510- 515 nm dalga boyunda ışıma yaptığı ve numunelerin elektromanyetik spektrumun UV ve görünür aralığında uyarıldığı görülmüştür. Ayrıca yanma reaksiyonu numunelerinin sol-jel numunelerinden daha şiddeti ışıma yaptığı; sol-jel numunelerinin ise katı hal numunelerinden daha şiddetli ışıdığı gözlemlenmiştir. Farklı sentez yöntemleri yapı içinde farklı hata merkezleri oluşturmuş bunun sonucunda katkısız ve aynı birleşimdeki örneklerin uyarılma eğrilerinde farklı dalga boylarında pikler gözlemlenmiştir. Aynı şekilde farklı katkılarla katkılanan numunelerin uyarılma eğrilerinde de farklı dalga boylarında pikler görülmüş ve her katkının yapıda farklı bir tuzak seviyesi oluşturduğu anlaşılmıştır. Bununla birlikte her bir katkı elementi

sentez metoduna bağlı olarak optik özelliklerde farklı değişime neden olmuş; genel olarak Y katkılı numuneler fosforesansı iyileştirirken diğer katkılar olumsuz etki yapmışlardır.

1. INTRODUCTION

Lighting needs of humans are very great in order to better protect themselves in the dark. They also need light to extend working hours and to entertain themselves in the night. To meet this need, people continually developed new lightening technologies from the early ages of human history. Illumination by light has evolved from wood fires to torch flames, burning of oil, candles, gas flames, incandescent lamps, fluorescent lamps, and light emitting diodes (LEDs), combined with photoluminescence (PL) from phosphor particles. These improvements in lighting technologies have a significant influence on living standards.

Like the lightening, the need to communicate with others became the reason for a significant change in technology. Communication techniques and technologies have progressed from faces of rock cliffs, to cave walls, clay tablets, parchment, wood and bamboo plates, sheets of paper, magnetic tapes, and electronic chips. The spread of information has significantly gained speed with the development of electronic devices. Since the information stored in electronic devices is invisible to the human eyes there was a need for the visualization of the invisible information. Therefore, display devices (FED, PDPs) have been developed as an interface between human and electronic devices. A significant proportion of luminescent materials are used in display devices to convert this invisible information [1].

Increasing demand for such electronic devices continues to exert pressure on an already stretched world energy infrastructure. Thus, there is a crucial need to develop energy-friendly, environmental-friendly luminescent materials with high luminous efficiency, high chromatic stability, brilliant color-rending properties, long persistence and low cost [2]. Long persistence phosphors which have glowing time from a few minutes to several hours after cutting of excitation source are one of the most used luminescence materials. This kind of long glowing radiation can be explained by recombination of the trapped electrons and thermally released holes. Suitable dopant ions and certain host materials are needed to obtain efficient phosphorescence [3].

For the last decades, a number of study on long persistence phosphors have been made. Firstly, ZnS-type phosphors especially ZnS:Cu, were found as a long phosphorescent phosphors and then it was used in a variety of applications. The next generation of long persistent phosphor compromised the alkali-earth sulfides, such as CaS and SrS which are known as Lenard's phosphors. Although excitability by sunlight is the main advantage of these phosphors, they do not have bright and long phosphorescence enough for many applications and they are chemically unstable. Additionally, H_2S is released when they are exposed to moisture [3, 4].

In 1996, Matsuzawa et al. [4] reported a new type of long persistent phosphor, $SrAl_2O_4:Eu^{2+}$, Dy^{3+} which is first studied in 1970s by Abbruscato et al. $SrAl_2O_4:Eu^{2+}$, Dy^{3+} is one of the long persistent phosphor with color purity, longer afterglow time, higher radiation intensity, and chemical, thermal and radiation stability than conventional sulfide based phosphors. [3, 4, 5]. All of these advantages makes $SrAl_2O_4:Eu^{2+}$, Dy^{3+} an effective material for PDPs and LEDs. They have a large application areas such as luminous paints on highways, airports, buildings and ceramic products, as well as textiles, the dial plates of luminous watches, warning and escape route signs, etc. [5, 6].

The long phosphorescence is strongly dependent on the host materials and dopant ions as mentioned above. The host material is important since it defines the environment of the dopant ions and determines the physical behavior of the material to external disturbances. Meanwhile, the dopant ion determines the color of the emission and also the time of the afterglow [7]. $SrAl_2O_4$ is preferred as a good host material for the emission of Eu^{2+} ions [8]. Co-doping has also strong influence on phosphorescence time and emission wavelength. There are many studies on how different co-doping ions with their different concentration affect the luminescence properties in $SrAl_2O_4:Eu^{2+}$, Dy^{3+} system such as $SrAl_2O_4$: Er^{3+}[9]; $SrAl_2O_4:Eu^{2+}$, Dy^{3+}, Gd^{3+}[10]; $SrAl_2O_4:Eu^{2+}$, Dy^{3+}, Tb^{3+}[5] etc.

This study aims to sensitize $SrAl_2O_4:Eu^{2+}$, Dy^{3+} phosphors with solid state, modified sol-gel and solution-combustion methods and investigate the nano size effects on phosphorescence characteristic of this phosphor. The effect of co-doping with Fe, Ni, Co and Y on the phosphorescence characteristic is also investigated.

2. LUMINESCENCE

2.1 Terminology

Before the word of “luminescence”, the word “phosphor” was invented in the early 17thcentury and it remained unchanged. The first known phosphor material was found by alchemist Vincentinus Casciarolo of Bologna, Italy. He found a heavy crystalline stone and fired it in a charcoal oven to convert it into a noble metal. He observed that sintered stone emits red light in the dark after exposure to sunlight. After this discovery, similar findings were reported from different places in Europe and these light-emitting stones were named as “phosphors” which means “light bearer” in Greek [3].

The word luminescence, which includes both fluorescence and phosphorescence, was introduced by Eilhardt Wiedemann, a German physicist, in 1888. This word originates from the Latin word *lumen*, light in English. The word phosphorescence, which means persisting light emission from a substance after the exciting radiation has removed, was derived from the word phosphor [3]. On the other hand, if the indistinct short after-glow occurs following excitation, this is named as fluorescence. This term was introduced to denote the ability of fluorspar (CaF_2) to change invisible light beyond the violet end of the visible spectrum into blue light by George Gabriel Stokes in 1852 [11].

Presently, the word luminescence is defined as light emission by a substance resulting from excitation of its electronic state with different energy source. Here, the word light includes the near-ultraviolet, visible region and the near-infrared regions of electromagnetic spectrum. Therefore, usage of the terms fluorescence and phosphorescence is different for organic and inorganic materials. For inorganic substances, light emission from a substance during the time when it is exposed to exciting radiation is called fluorescence, while the after-glow if detectable by the human eye after the cutting of excitation is called phosphorescence. For organics,

light emission from a singlet excited state is called fluorescence, while it is from a triplet excited state is defined as phosphorescence [1].

2.2 Theory of Luminescence

Luminescence is most conveniently defined as the radiation emitted by a molecule, or an atom, after it had absorbed energy to go to an exited state. The main types of luminescence are consisting of fluorescence and phosphorescence. Luminescence mechanism of a material is strongly related with its electronic states [12].

Electronic states of molecules can be grouped into two broad categories, singlet states and triplet states. The terminologies singlet and triplet state are the result of the spin quantum numbers (figure 2.1). Singlet spin state is formed when a pair of electrons occupying the same electronic ground state has opposite spins. In the ground state, all molecules except oxygen are in the singlet form. By the way, triplet states are those in which one set of electron spin have become unpaired. Triplet states and singlet states differ significantly in their properties as well as in their energies. A triplet state always lie lower in energy than its corresponding singlet state [12, 13, 14].

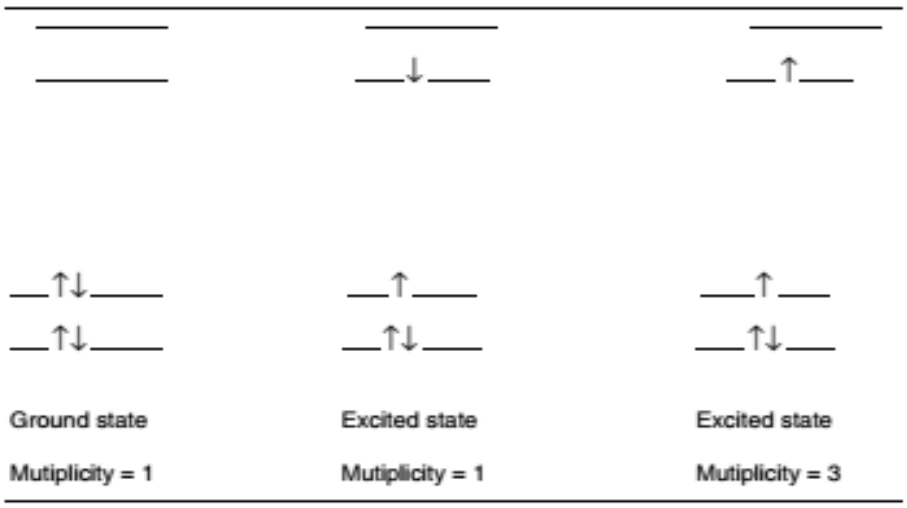

Figure 2.1: Spin configurations of the singlet and triplet states [14].

A valance electron of a molecule or an atom is excited from its ground state to an excited state with conservation of the electron's spin when a visible or UV photon is absorbed. Absorbing a photon promotes one of the electrons to a singlet excited state. This phenomenon is called "excitation". After random time from excitation, the electron spontaneously turns back to the ground state. This return process is called

decay, deactivation or relaxation. This relaxation process can occur in two different ways; radiative and non-radiative.

Fluorescence and phosphorescence are two different types of radiative relaxation. If there is a photon emission while relaxation takes place, this type of relaxation is called radiative relaxation. Fluorescence is observed when emission of a photon takes place from a singlet excited state to a singlet ground state or between any two energy levels with the same spin. The obtaining possibility of a fluorescent transition is very high. As a result of the average lifetime of the electron in the excited state is only 10^{-5}–10^{-8} seconds, fluorescence decays rapidly after the excitation source is removed.

In some cases an electron in a singlet excited state is transformed to a triplet excited state in which its spin is no longer paired with that of the ground state. Emission between a triplet excited state and a singlet ground state or between any two energy levels that differ in their respective spin states is called phosphorescence. Because the average lifetime for phosphorescence ranges from 10^{-4} to 10^{4} seconds, phosphorescence may continue for some time after removing the excitation source [12, 13].

Electronic states of a molecule and transitions between them are illustrated by a Jablonski Diagram which is first proposed by Professor Alexander Jablonski in 1935 to describe absorption and emission of light (figure 2.2). At the present, modified Jablonski Diagrams are frequently used and are actually state diagrams. In this diagram, molecular electronic states are represented by horizontal lines displaced vertically to indicate relative energies. They are also grouped according to multiplicity into horizontally displaced columns. A parameter called the multiplicity (M) is defined as

$$M=|s1+s2|+1 \qquad \textbf{(2.1)}$$

When the spins are parallel, i.e., M=1, we have a singlet state S_n. When the spins are anti-parallel, i.e., M=3, we have a triplet state T_n. Excitation and relaxation processes that interconvert states are indicated in the diagrams by arrows. Radiative transitions are generally indicated with straight arrows while non-radiative transitions are generally indicated with wavy arrows [15].

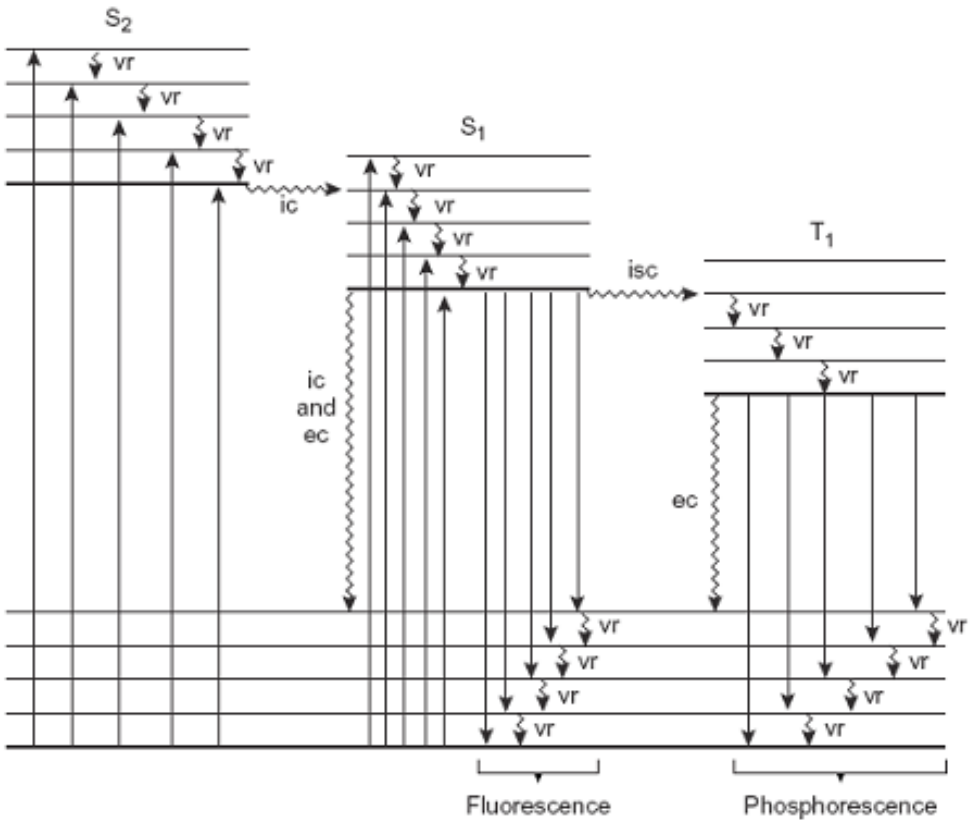

Figure 2.2 : Jablonski Diagram [13].

Vibrational relaxation (VR), internal and external conversion, intersystem crossing are types of non-radiative relaxation. In vibrational relaxation, an electron in an excited vibrational energy level loses energy while it moves to a lower vibrational energy level in the same electronic state. Vibrational relaxation is very rapid. This means that before an excited molecule in a solution can emit a photon, it will undergo vibrational relaxation, and therefore photon emission will always occur from the lowest vibrational level of an excited state.

Internal conversion (IC) occurs when a molecule in the ground vibrational level of an excited electronic state passes directly into a high vibrational energy level of a lower energy electronic state of the same spin state. By a combination of internal conversions and vibrational relaxations, a molecule in an excited electronic state may return to the ground electronic state without emitting a photon which is called as external conversion (EC). The last form of non-radiative relaxation is an intersystem crossing (ISC) in which a molecule in the ground vibrational energy level of an excited electronic state passes into a high vibrational energy level of a lower energy electronic energy state with a different spin state [12, 13].

2.3 Classes of Luminescence

Luminescence can be obtained as a result of excitation of a substance by many types of energy. Depending on the type of excitation source, luminescence is classified into several groups. These are photoluminescence (excitation by photons), cathodoluminescence (by cathode rays or energetic electrons), electroluminescence (by an electric field), triboluminescence (subject of a mechanical force) and chemiluminescence (by utilizing chemical reaction energy) [16].

Photoluminescence (PL) is caused by moving electrons to energetically higher levels through the absorption of photons. PL is a very useful tool in examining excitation transport in molecular solids, regular crystals or disordered system, and is a well-established technique to study optical properties and electronic structure of semiconductors. This type of luminescence includes two subtypes; fluorescence and phosphorescence. Fluorescence occurs as a result of singlet-singlet electronic relaxations after excitation source cut off and typical life time is nanoseconds. On the other hand, phosphorescence occurs as a result of triplet-singlet electronic relaxations and typical lifetime is from millisecond to hours period [1, 16, 17, 18].

Cathodoluminescence is the emission of photons which may have wavelengths in the visible spectrum as a result of impacting an electron beam on a luminescent material such as a phosphor. Due to this mechanism, it can be said that cathodoluminescence is the inverse of the photoelectric effect. The formation of images on television that uses cathode ray tube is due to cathodoluminescence. Many crystalline phosphors which are not luminescent under photo-excitation exhibit emission under the excitation by energetic electrons and the whole crystal lattice is strongly disturbed, and even electrons of the inner atomic shells of the luminescent centers are excited.

Electroluminescence is an optical and electrical phenomenon in which a material emits light in response to the passage of an electric current or to a strong electric field. Electroluminescence is the result of radiative recombination of electrons and holes in a material, usually a semiconductor. The excited electrons release their energy as photons.

Triboluminescence is phosphorescence that is triggered by mechanical action or electroluminescence excited by electricity generated by mechanical action. Some minerals glow when they were hit or scratched.

Chemiluminescence is luminescence where the energy is supplied by chemical reactions. Those glow-in-the-dark plastic tubes sold in amusement parks are examples of chemiluminescence. The energy needed comes from the reaction enthalpy. The reaction produces some new molecule that can have its electrons in an exited state right after it was formed. Decay to a ground state may then produce visible light or release the energy in some other way.

2.4 Long Persistent Phosphors

Obtaining persistent phosphors with different emission and excitation wavelength is the main aim of researching new phosphorescent materials. Since the beginning of 20^{th} century, studies of development new phosphor materials gained speed. For many decades, sulfide based phosphors are used such as CaS:Bi (which emits light of violet blue), CaSrS:Bi (which emits light of blue), ZnS:Cu (which emits light of green) etc. [6]. Zinc sulfide (ZnS) doped with copper ($ZnS:Cu^{+}$), was the most known and widely used persistent green light emitting phosphor which have persistent times as long as 40 minutes. Additionally, a number ofstudies are made to develop the persistent time such as, co-doping $ZnS:Cu^{+}$ with Co^{2+} doubled the persistence time of the Zn compound [20]. Many ZnS based persistent phosphors have been developed which have found uses as night vision materials. The main advantage of these phosphors is that they can be excited by sunlight. Their major disadvantage, however, is that they were chemically unstable and H_2S is released when they are radiated by ultraviolet radiation in the presence of moisture and thus reduces the luminescence. This disadvantage limits the usage of this phosphor at outdoors and under direct sunlight [6].

In 1996 T. Matsuzawa et al. [4] reported a new type of long-persistent phosphor $SrAl_2O_4:Eu^{2+},Dy^{3+}$ with a strong emission at 520 nm (green), which is developed from a phosphor $SrAl_2O_4:Eu^{2+}$ found by V. Abbruscato in 1971. The persistence time of $SrAl_2O_4:Eu^{2+},Dy^{3+}$ was extended to longer than 16 hours after co-doping with Dy^{3+} which is much longer lifetime compared to ZnS:Cu, Co (figure 2.3).Compared with sulfide phosphorescent phosphors, $SrAl_2O_4:Eu^{2+},Dy^{3+}$ possesses safer,

chemically stable, very bright and long-lasting photoluminescence which results in an unexpectedly large field of applications, such as luminous paints in highway, airport, buildings and ceramics products, as well as in textile, the dial plate of glow watch, warning signs and escape routine, etc. [21].

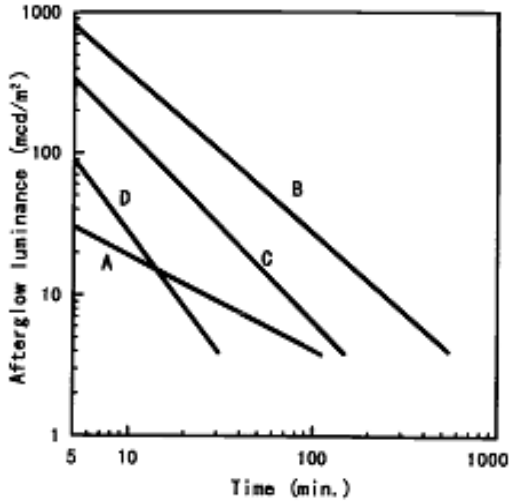

Figure 2.3 : Phosphorescence characteristics of A: $SrAl_2O_4:Eu^{2+}$, B: $SrAl_2O_4:Eu^{2+}$, Dy^{3+}; C: $SrAl_2O_4:Eu^{2+}$, Nd^{3+}; D: commercially ZnS: Cu, Co [4].

Discovery of Matsuzawa et al. marked the beginning of a renewed search for different and better persistent luminescent materials. Initially, this research was concentrated on alkaline earth aluminates and it took a few years before other types of compounds came into view. Many new long persistent phosphors have been found in past 10 years such as alkali-earth aluminates doped with Ce^{3+}, Mn^{2+}, and Tb^{3+}; alkali-earth silicates doped with Mn^{2+}, or Eu^{2+}/Dy^{3+}; alkali-earth oxide doped with Eu^{3+} rare-earth oxides and oxysulfides doped with Er^{3+}, Eu^{3+}, Ti^{4+} and Mg^{2+}; and other systems such as Zn phosphate doped with Mn^{2+} [20]. In table 2.1, some aluminate and silicate based long persistent phosphors are shown [22].

Table 2.1 : Some of known long persistent phosphor compounds [21].

	Host Material	**Dopants**	**Emission Max.**	**Afterglow Max.**	**Afterglow Duration**
Aluminates	$SrAl_2O_4$	Eu^{2+},Dy^{3+}	520 (green)	idem	>30 h
	$CaAl_2O_4$	Eu^{2+},Nd^{3+}	440 (blue)	430 (blue)	>5 h
	$BaAl_2O_4$	Eu^{2+}, Dy^{3+}	500 (green)	idem	>2 h
	$Sr_4Al_{14}O_{25}$	Eu^{2+}, Dy^{3+}	490 (blue)	idem	>20 h
Silicates	$Sr_2MgSi_2O_7$	Eu^{2+}, Dy^{3+}	470 (blue)	idem	>10 h
	$Ca_2MgSi_2O_7$	Eu^{2+}, (Tb^{3+})	515 /535 (green)	idem	>5 h
	$Ba_2MgSi_2O_7$	Eu^{2+}, Tm^{3+}	505 (green)	idem	>5 h

2.4.1 Strontium aluminate

$SrAl_2O_4$ is known one of the best matrix materials for long lasting green emission of Eu^{2+} ions. In the $SrO\text{-}Al_2O_3$ system (figure 2.4), there are four intermediate compounds; $Sr_3Al_2O_6$, $SrAl_2O_4$, $SrAl_4O_7$, $SrAl_{12}O_{19}$ [23]. We can obtain desired composition by varying temperature and the molar ratio of SrO and Al_2O_3.

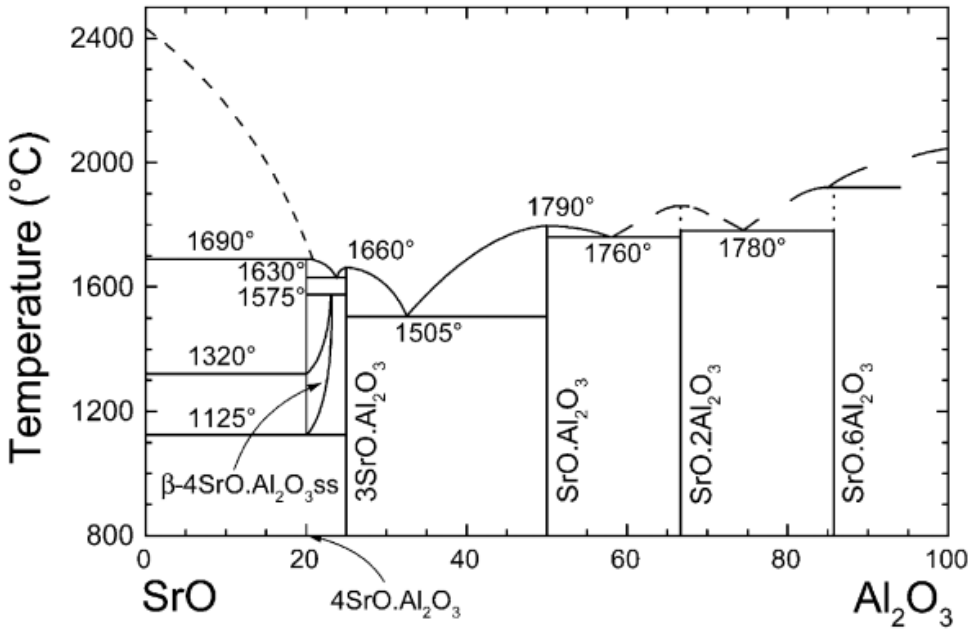

Figure 2.4 : $SrO\text{-}Al_2O_3$ phase diagram [22].

The $SrAl_2O_4$ exists in two crystallographic forms and a reversible transition between them occurs at 650°C. The structure of the low-temperature phase is monoclinic (space group $P2_1$, a = 8.447 Å, b = 8.816 Å, c = 5.163Å and $\alpha = \Upsilon = 90^o$) (figure 2.5 [25]) and the high temperature phase is hexagonal (space group $P6_{322}$). The monoclinic $SrAl_2O_4$ is formed by a three-dimensional framework of corner-sharing AlO_4 tetrahedron. The each oxygen is shared with two aluminum ions so that each tetrahedron has one net negative charge that balanced by the large divalent cations that occupy two different interstitial sites within the tetrahedron framework [26]. Monoclinic $SrAl_2O_4$ structure is shown according to a and c directions in figure 2.6 [24].

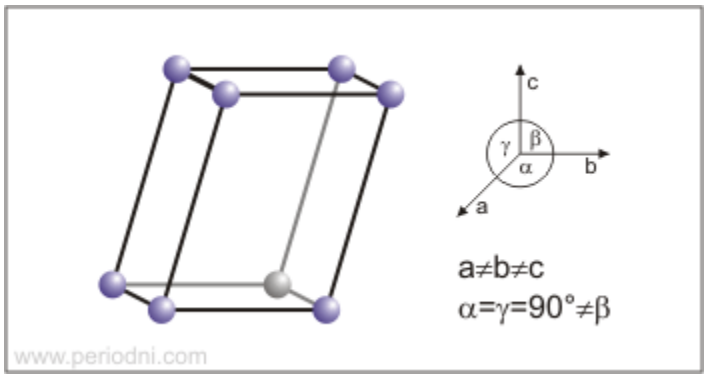

Figure 2.5 : Monoclinic $SrAl_2O_4$ structure [25].

There are two crystallographically different sites for Sr^{2+}, which have identical coordination numbers. The two environments differ only by a slight distortion of their square planes. The Sr^{2+} and Eu^{2+} ions are very similar in their ionic size (i.e., 1.21 and 1.20 A˚, respectively). Consequently, when occupied by Eu^{2+} ions, the two different Sr^{2+} sites will have a quite similar local distortion, so that the Eu^{2+}ions located at the two different Sr^{2+} sites will have very similar local environments. The second dopant Dy^{3+} ion (0,97A˚) also occupies the Sr^{2+} site [8, 9, 23].

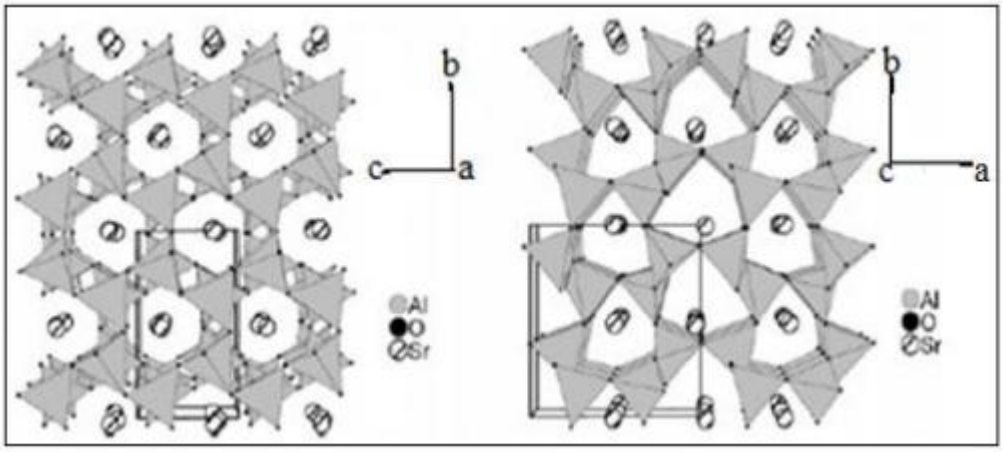

Figure 2.6 : Representation of monoclinic $SrAl_2O_4$ structure along the a and c directions [23].

2.4.2 Long persistence mechanism

With the discovery of the long persistent phosphor properties of $SrAl_2O_4:Eu^{2+}$, Dy^{3+}, the long phosphorescence mechanism became a subject of curiosity. Although relatively little research had been done on this subject, there have been reported several models. In all of these models, Eu^{2+} ions are accepted as the luminescent centers and the photo-excited luminescence is considered to be due the transition from 5d level to 4f level of Eu^{2+}. Therefore, long persistent is thought a result of the

trapped–detrapped process. It was generally agreed upon that after excitation, charge carriers could get caught by so-called traps, energy levels inside the forbidden band gap with a very long lifetime. The charge carriers are only gradually released from these traps, when they can return to the activators and produce luminescence [4, 21, 26]. Here several models are given briefly:

- The Matsuzawa model

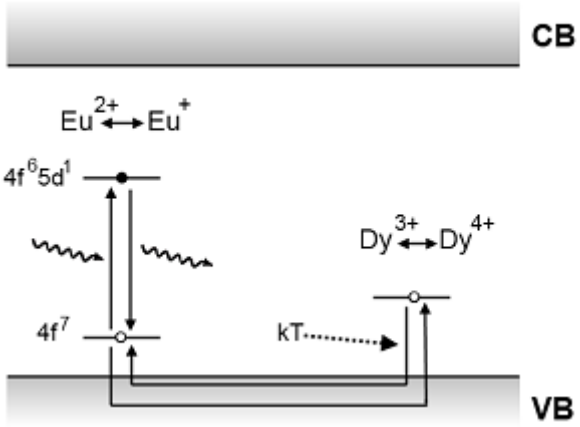

Figure 2.7 : Persistent luminescence mechanism proposed by Matsuzawa et al. for $SrAl_2O_4:Eu^{2+}$, Dy^{3+} [21].

Matsuyama *et al*. tried to explain the origins of the great persistent luminescence in the same article announcing the discovery of $SrAl_2O_4:Eu^{2+}$, Dy^{3+}. The Matsuzawa model modified Abbruscato's assumptions in order to explain the influence of rare earth co-doping. In this model, holes are assumed to be the main charge carriers (figure 2.7). When a Eu^{2+} ion is excited by an incident photon, there is a possibility that a hole escapes to the valence band, thereby leaving behind a Eu^{+} ion. The hole is then captured by a trivalent rare earth ion, such as Dy^{3+}, thus creating a Dy^{4+} ion. After a while, thermal energy causes the trapped hole to be released into the valence band again. From there it can move back to a Eu^{+} ion, allowing it to return to the Eu^{2+} ground state with emission of a photon [4].

- The Aitasalo model

In 2003, Aitasalo et al. suggested a model that differed considerably from the Matsuzawa model (figure 2.8). In this model, electrons are excited directly from the valence band into trap levels of undefined origin. The hole that is created in this way migrates towards a calcium vacancy where it is caught. The trapped electron is removed from the trap level by thermal energy and stops at an oxygen vacancy level.

Released energy due to recombination of trapped electrons and holes is not enough to transfer electron to conduction band so this energy is delivered directly to the europium ions via energy transfer. According to this assumption, close proximity of the vacancies to the luminescent centers is required. The transferred energy excites an electron of europium to a 5d level, followed by recombination and emission of the persistent luminescent light [27].

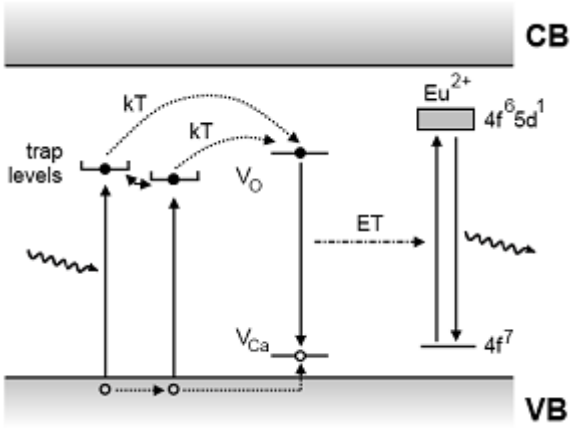

Figure 2.8 : Persistent luminescence mechanism proposed by Aitasalo et al. for $CaAl_2O_4:Eu^{2+}, Dy^{3+}$ [21].

The Aitasalo model was introduced for several reasons. Firstly, the Matsuzawa model ignored the observed persistent luminescence in un-co-doped $SrAl_2O_4:Eu^{2+}$. And second reason is the difficulty of the occurrence of monovalent europium and tetravalent dysprosium ions in the material which are used in the Matsuzawa model [21, 27].

- The Dorenbos model

Dorenbos made a number of studies to determine of lanthanide energy levels in inorganic compounds with applications in scintillator physics and persistent luminescence. Some problems with the Matsuzawa model encouraged Dorenbos to present a different model in 2005, depicted in figure 2.9. The first problem is that, as mentioned above, the existence of Eu^+ and Dy^{4+} in aluminate or silicate compounds is highly impossible. And the second reason is that the assumed hole on the ground state of Eu^{2+} after excitation is based on faulty reasoning. Because, the energy levels of the lanthanides are localized and the 4f state of europium after the excitation should not be interpreted as a real hole that can accept an electron [28, 29].

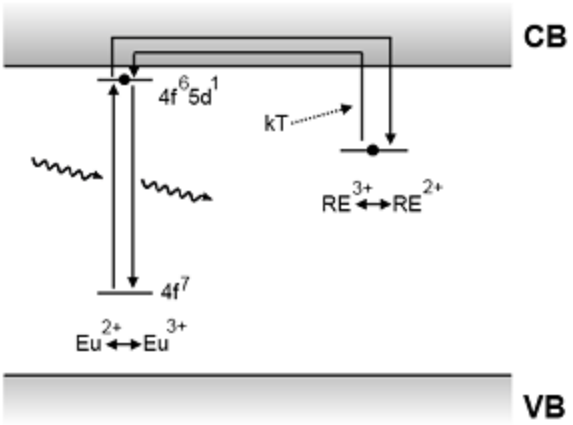

Figure 2.9 : Persistent luminescence mechanism proposed by Dorenbos et al. for aluminate and silicate compounds [21].

In the Dorenbos model, since the 5d level of divalent europium lies very close to the conduction band, these excited electrons can easily be passed through into the conduction band and subsequently caught by a trivalent rare earth co-dopant, creating a divalent ion. Thermal energy can then release the trapped electron, after which it recombines upon reaching a luminescent center [28, 30]. This mechanism is basically the same as the one suggested by Matsuzawa, but it does not require the existence of Eu^{+} and RE^{4+}. It cannot, however, explain the existence of intrinsic persistent luminescence in un-co-doped materials.

- The Clabau model

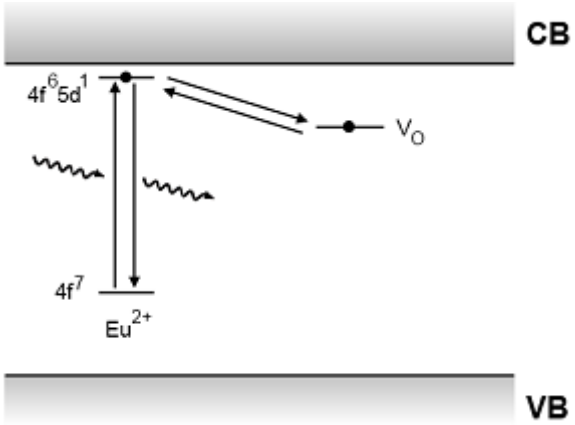

Figure 2.10 : Persistent luminescence mechanism proposed by Clabau et al. for $SrAl_2O_4:Eu^{2+}, Dy^{3+}$ [21].

Clabau et al. did not accept the Matsuzawa model for the same reasons as Dorenbos and they developed a new model for persistent luminescence which is shown in figure 2.10. Their model is similar to the Dorenbos model, but differs on some

important points. Firstly, there is no migration of electrons through the conduction band. The transport of electrons between the traps and the luminescent centers is believed to occur through direct transfer, which requires close proximity between the europium ions and the lattice defects [31, 32].

A second difference to the Dorenbos mechanism is the nature of the traps. Clabau et al. noticed that the relevant peaks differed in size and location, but they were very similar in shape by comparing to glow curves of un-co-doped and Dy^{3+} co-doped $SrAl_2O_4:Eu^{2+}$. So they concluded that the chemical nature of the trap was not influenced under co-doping. This led them to the idea that lattice defects, namely oxygen vacancies, must act as traps in $SrAl_2O_4:Eu^{2+}$, RE^{3+} [32].

- Recent developments

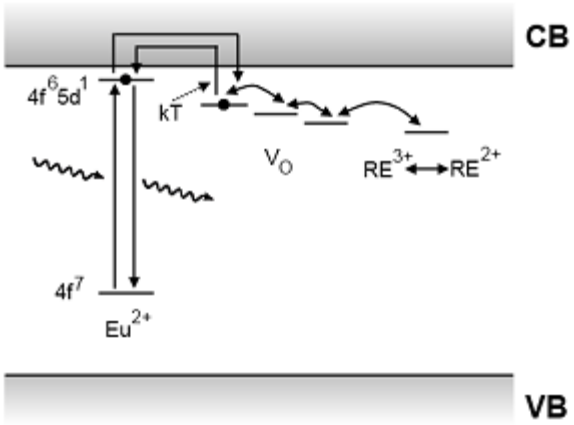

Figure 2.11 : Persistent luminescence mechanism proposed in 2006 by Aitasalo et al. for $CaAl_2O_4:Eu^{2+}$, Dy^{3+} [21].

Aitasalo et al. described a mechanism for persistent luminescence in 2006 (figure 2.11). This model incorporates suggestions from both Clabau and Dorenbos [33]. In this model, electrons that are excited in the Eu^{2+}luminescent centers can easily escape into the conduction band. Both oxygen vacancies and trivalent co-dopant ions introduce trap levels. When enough thermal energy is available, the captured electrons can escape again into the conduction band and recombine in a luminescent center.

2.4.3 Fabrication methods

$SrAl_2O_4:Eu^{2+}Dy^{+3}$ phosphor has been achieved by several methods such as solid-state reactions, sol–gel techniques, combustion synthesis, microwave-accelerated

hydrothermal technique, laser ablation, and microemulsion method etc. Among these the most commonly used ones are the solid state reaction method, modified sol-gel, and combustion techniques. These techniques are easy to apply and economically viable since they do not need expensive equipments. In this part these fabrication techniques are briefly explained.

2.4.3.1 Solid state reaction method

The solid-state reaction (SSR) is a widely used method to prepare polycrystalline solids from a mixture of solid starting materials. It is performed at high temperatures, typically around 1600°C, because of the refractory nature of the precursors. Reaction conditions, structural properties of the reactants, surface area of the solids, their reactivity are such important parameters which have high influence on SSR.

The SSR is also used to synthesize well-reacted, small (micrometer level) particle size phosphors. Generally $SrCO_3$, Al_2O_3, Eu_2O_3 and Dy_2O_3 are used as starting materials with specific stoichiometric ratios in this method. Also, $Eu(NO_3)_3$ and $Dy(NO_3)_3$ used as starting materials [34]. Small amount of boric acid or boron oxide could use as flux material to reduce sintering temperature, modify particle size and improve the luminescence properties. To produce a homogeneous mixture, these materials are mixed using a planetary mill for several times in ethanol medium. After mixing, ethanol is removed from the mixture, and obtained powders are sintered at 1200-1350°C.

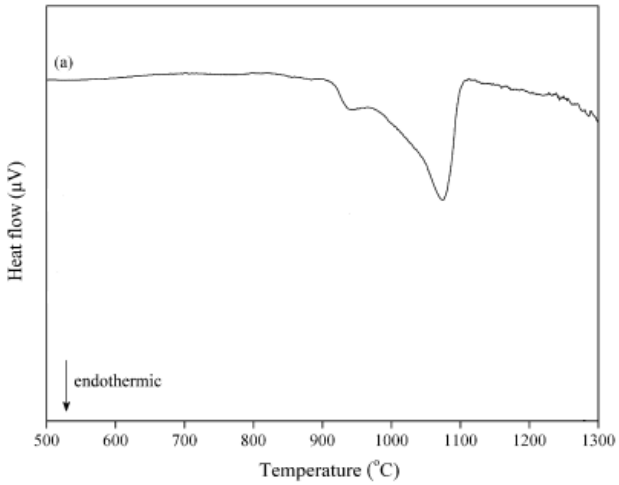

Figure 2.12 : DTA curves of the un-calcined mixture of $SrAl_2O_4:Eu^{2+}$, Dy^{3+} [35].

In figure 2.12, DTA curve which is obtained from a carbonate and oxide mixture is represented. There are two endothermic peaks at 920°C and 1100°C due to

polymorphic phase transformation and decomposition of $SrCO_3$ respectively [35]. The temperature above 1300°C, the reaction occurs between oxides and $SrAl_2O_4$ phase is obtained. Because of the Eu^{2+} is emitting center in this phosphors, a reducing atmosphere (H_2/N_2 or active carbon) are used to reduce the Eu^{3+} ions to Eu^{2+} ions during the thermal treatments in the most of reports [6, 34, 35].

2.4.3.2 Sol-gel method

The sol-gel technique is the general name given to the production of fine ceramic powders ceramic, glasses and composite materials from the basis of the their solution. Sol means a stable suspension of colloidal solid particles or polymers in a liquid and gel means porous, three-dimensional, continuous solid network surrounding a continuous liquid phase.

The sol–gel process is used efficiently for the syntheses of phosphors due to the good mixing of starting materials and relatively low reaction temperature resulting in more homogeneous products than those obtained by solid-state reaction synthesis method. The direct solid-state preparation of monoclinic MAl_2O_4 is usually carried out at around 1300°C due to impurities such as $M_3Al_2O_6$ are formed at lower temperatures. A lower temperature (900°C) has been reported for the successful preparation of MAl_2O_4 (M: Mg, Co, Ca, Sr and Ba, etc.) ultra-fine (nanometer level) powders by sol–gel technique [26].

Generally $Sr(NO_3)_3$, $Al_2(NO_3)_2.9H_2O$, , $Eu(NO_3)_3$ and $Dy(NO_3)_3$ are used as starting materials with specific stoichiometric ratios in this method. The nitrate precursors are added to distilled water and continuous stirring is at about 100°C is carried out to obtain homogeneous sol mixture. Small amount of boric acid is used as flux material to reduce sintering temperature, modify particle size and improve the luminescence properties. Additionally, citric acid (CA) is added as chelating agent (cross-linking) to boiling water at the ratio of 2:1 of CA to total metal ions in the solution. By keeping the solution at 100°C for 2 h under constant stirring, the solution becomes viscous. After the sol was dried at 200°C for 12 h, brown dried-gels were obtained. The dried-gels were calcined at 800°C in air atmosphere for 6 h to remove the residual carbon. Finally, the calcined powders were sintered up to 1300°C for 2,5 h in reducing atmosphere [37].Here there are some advantages of the sol-gel methods [19]:

- High homogeneity of the chemical composition of the materials produced. Molecule-level homogeneous multicomponent materials can be obtained.
- High uniformity of doping ion distribution. No “local” concentration quenching will occur because of impurity clustering and higher doping concentration becomes possible.
- Processing temperature can be very low. This allows the doping of fragile organic and biological molecules into porous inorganic materials and the fabrication of organic–inorganic hybrid materials.
- The microstructure (porosity and size of pores) of the materials can be controlled. Nanoscale uniform pores can be obtained at intermediate processing temperatures while high-density materials can be produced with higher annealing temperature.
- The sol–gel procedures produce little unintentional contamination. No milling and grinding are needed, as these processes are known to contaminate samples.

2.4.3.3 Combustion method

The term ‘combustion’ covers flaming and smoldering as well as explosive reactions. Combustion synthesis is an important powder processing technique generally used to produce complex oxide ceramics such as aluminates, ferrites, and chromites. It involves the exothermic reaction between metal nitrates and a fuel, typically urea (CH_4N_2O), carbohydrazide (CH_6N_4O), or glycine ($C_2H_5NO_2$) [38].

The technique is required only appropriate raw materials and a muffle furnace or a hot plate at temperatures of 800°C or less, much lower than the phase transition of the target material. In a typical combustion reaction, the precursor mixture of water, metal nitrates, and fuel decomposes, dehydrates, and breaks away into a flame after about 3–5 min. The chemical energy released from the exothermic reaction between the metal nitrates and fuel can rapidly heat the system to high temperatures (>1600°C) without an external heat source. The resultant product is a voluminous, foamy powder which occupies the entire volume of the reaction vessel [38]. Combustion synthesized powders are generally more homogeneous, have fewer impurities, and have higher surface areas than powders prepared by conventional solid-state methods. The parameters that influence the reaction include: type of fuel,

fuel to oxidizer ratio, use of excess oxidizer, ignition temperature, and water content of the precursor mixture [39].

Table 2.2 : Number of moles of gas produced for different fuels per mole of metal sesquioxide formed [39].

Fuel	Reaction	No. of moles of gas produced
Glycine	$2M(NO_3)_3 + 10/3C_2H_2NO_2 \longrightarrow M_2O_3 + 20/3CO_2 + 25/3H_2O + 14/3N_2$	19,7
Urea	$2M(NO_3)_3 + 5CH_4N_2O \longrightarrow M_2O_3 + 5CO_2 + 10H_2O + 8N_2$	23,0
Carbohydrazide	$2M(NO_3)_3 + 15/4CH_4N_4O \longrightarrow M_2O_3 + 15/4CO_2 + 45/4H_2O + 21/2N_2$	25,5

In table 2.2, it is shown that when the combustion occurs completely, the obtained gaseous products are only N_2, CO_2, and H_2O with different amounts due to different fuel types. The generation of gaseous products creates micro- and nano-porous regions in the sample which increase the surface area of the powders. Additionally, according to McKittrick et al. type of fuel used is caused difference in particle size due to the number of moles of gaseous products released during combustion. As more gases are released, the agglomeration is eliminated and more heat is carried from the system thereby blocking particle growth. A greater number of moles of gas are produced in combustion reactions with carbohydrazide [39].

Yu et al.[40] made a case study to produce $SrAl_2O_4:Eu^{2+}$ nano-particle phosphor by combustion method with the $SrAl_2O_4$:0:1Eu formula and the combustion reaction urea is described by the following equation:

$$2(Al(NO_3)_3 \cdot 9H_2O) + Sr(NO_3)_2 \cdot 4H_2O + m(CO(NH_2)_2 + 1.5mO_2 = SrAl_2O_4 + (22+2m)H_2O + (4+m)N_2 + 10O_2 + mCO_2 \quad \textbf{(2.2)}$$

They reported that the processing method may avoid the use of H_2 atmosphere during the thermal treatments since the organic matter generated during the combustion of the gel itself produces the reducing atmosphere. It is evidence that they did not find any characteristic peaks of the Eu^{3+} in the emission spectra. But we did not see any emission peaks of Eu^{3+} in our combustion samples. On the other hand, the radius of Eu^{2+} is 117 pm, which is similar to that of Sr^{2+}, 118 pm. So it is expected that Eu^{2+} often occupies the lattice of Sr^{2+} ion in the host and this substitution may finally give new Eu(II) compound.

According to their study, the optimum ratio of urea is 1.5 which gives the in the combustion synthesis of nano-$SrAl_2O_4$ phosphors. When the ratio of urea is higher than 1.5, the produced heat is not favorable for forming the $SrAl_2O_4:Eu^{2+}$ of single-phase monoclinic structure. On the other hand, when the concentration of the urea is too low, the reactive temperature will be lower, which will lead to the uncompleted reaction of raw materials. Additionally, initiating temperature and time also have significant role on grain size which becomes larger while increasing the time and the temperature.

2.4.4 Effect of addition of boric acid on luminescence properties

Phosphors with high luminous intensity, excellent chemical and thermal stability are desired for many applications, especially for the display devices. [41,42]. Morphology and uniform particle size have an extraordinary importance on luminescence intensity and stability of phosphors. Especially sphere-like morphology can give a high packing density and minimize light-scattering, whereas uniform particle size can yield high-quality screen surface [43].

Production method and flux materials are decisive factors to determine sphere-like morphology, particle size, and size distribution. Although there are several methods such as spray pyrolysis, solvothermal, and hydrothermal method to prepare phosphor with spherical shape and uniform size, these methods have disadvantages such as low yield, expensive equipments, and high environmental loads [10].

Using of flux in synthesis methods provides highly crystallized and chemically homogeneous powder particles with controllable morphology and size at a temperature below the melting point of reactants. Thus, flux behaves like “shape modifier” in synthesis of phosphors by accelerating the chemical reaction with reducing the required temperature. Besides, addition of flux material until certain amounts significantly improves luminescence properties of phosphors. There are various types of flux material such as NH_4Cl, NH_4F, H_3BO_3, LiF, NaF. These flux materials have advantages such as low melting points, good chemical stability, and easy removal from products [43].

In the literature, boric acid (H_3BO_3) is mostly used flux material in $SrAl_2O_4$ based phosphors. Boric acid is soluble in boiling water. When heated above 170 °C, it dehydrates, forming metaboric acid (HBO_2):

$$H_3BO_3 \rightarrow HBO_2 + H_2O \quad \textbf{(2.3)}$$

Metaboric acid is a white, cubic crystalline solid and it is only slightly soluble in water. It melts at about 236°C and when heated above about 300°C further dehydrates, forming tetraboric acid or pyroboric acid ($H_2B_4O_7$):

$$4\ HBO_2 \rightarrow H_2B_4O_7 + H_2O \quad \textbf{(2.4)}$$

Further heating leads toboron trioxide (B_2O_3). B_2O_3 melts at 450 or 510 °C depending on its crystalline structure and boils 1800 °C.

$$H_2B_4O_7 \rightarrow 2\ B_2O_3 + H_2O \quad \textbf{(2.5)}$$

H_3BO_3 act as an inert high temperature solvent medium (flux); it actively participates in reactions and, depending upon the H_3BO_3 concentration, different phases can be stabilized such as $SrAl_2O_4$, $Sr_4Al_{14}O_{25}$ and $SrAl_{12}O_{19}$. In table 2.3, it is shown that the final product is dependent on the $SrO/Al_2O_3/B_2O_3$ ratio [44].

Table2.3 : Compositions of strontium aluminate samples and obtained phase.

Sample	Nominal SrO / Al_2O_3 / B_2O_3 ratio (Sr / Eu / Dy = 1: 0.01: 0.02)	Phase identification by XRD
$SAEDB_0$	1:1:0	$SrAl_2O_4$
$SAEDB_{0,05}$	1:1:0.05	$SrAl_2O_4$
$SAEDB_{0,2}$	1:1:0.2	$SrAl_2O_4$ (major) and $Sr_4Al_{14}O_{25}$ (minor)
$SAEDB_{0,4}$	1:1:0.4	$Sr_4Al_{14}O_{25}$
$SAEDB_{1,0}$	1:1:1	$SrAl_2B_2O_7$

According to Matsuzawa et al. [6], it is possible to add 1-10% by weight of boric acid as flux to starting material. If the amount of flux is less than 1% by weight, the effect of flux vanishes and if the amount of flux is more than 10 % by weight, flux is solidified so that there will be different phases and the product becomes very hard to mill and sieve which may be required later. They used 0,08mol (2,5 % by weight) H_3BO_3 to synthesize $SrAl_2O_4$ based phosphor in SSR.

Therefore, Faridnia et al. reported that large amount of boric oxide (>5 mol %) reacts with alumina and produces an amorphous aluminum borate phase which consumes Al, then a crystalline phase ($Sr_5Al_2O_8$) is formed. Also, according to them, it seems that with the increase of B_2O_3 concentration, $Sr_5Al_2O_8$ appears as the major phase and $SrAl_2O_4$ remains as a minor phase [8].

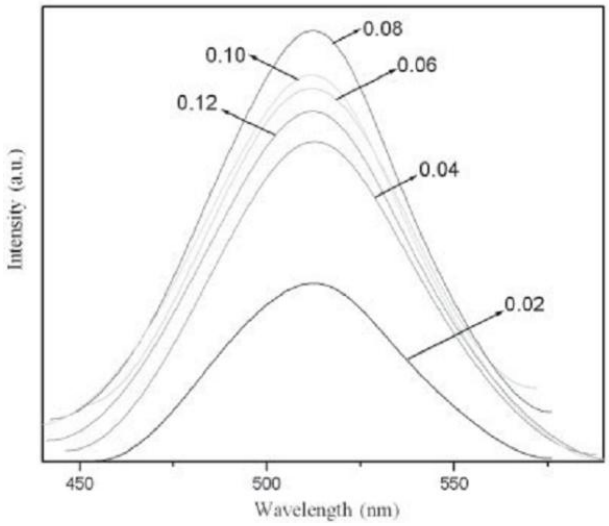

Figure 2.13 : Emission spectra of samples at various molar fractions of boric acid [5].

Song et al. studied the effect of different boric acid molar fractions (0.02, 0.04, 0.06, 0.08, 0.10 and 0.12) on the emission spectra of phosphors which is produced by combustion technique. The effect of H_3BO_3 can be seen in the figure 2.13 that the emission spectra are broad but symmetrical bands peak at 513 nm (excitation at 335 nm). The shapes and positions of the bands remain the same irrespective of the boric acid content, whereas the intensity varies with increasing boric acid concentration. Clearly, when the molar fraction of boric acid is 0.08, the phosphor shows the highest emission intensity [5].

2.4.5 Size dependence of luminescence properties

The luminescent properties of most luminescent materials are greatly dependent on the grain size. When the grain size reaches nanometer grade, the luminescent materials will show some attractive properties, such as the blue shift of excitation and emission spectra.

As mentioned above, the grain size of phosphor powders prepared through solid-state reaction method is in several tens of micrometers [34]. Phosphors of small particles must be obtained by grinding the larger phosphor particles. Those processes easily introduce additional defects and greatly reduce luminescence efficiency. With the development of scientific technologies on materials, several chemical synthesis techniques, sol–gel [26], combustion synthesis [35] methods, have been applied to prepare nano sized $SrAl_2O_4$ phosphors. All of these methods were conducted in

liquid phases so that each component can be accurately controlled and uniformly mixed [21].

Tang and Zhang et al. [45] studied the size dependency of phosphorescent characteristic of $SrAl_2O_4$: Eu^{2+}, Dy^{3+} phosphors. They prepared the materials by sol-gel and solid state reaction methods. According to their results, the grain sizes of gel samples are in nanometer range while the grain size of solid state reaction samples is micrometer range and it is observed that the grain sizes of gel samples increase (from 26 to 90 nm) with the increasing sintering temperature (from 800 to 1380°C for 2 hours). Additionally, they observed that although emission and excitation spectra of this phosphor have a similar shape, there are blue shifts in emission and excitation spectra of this phosphor (figure 2.14 and 2.15, respectively) while grain size decreases.

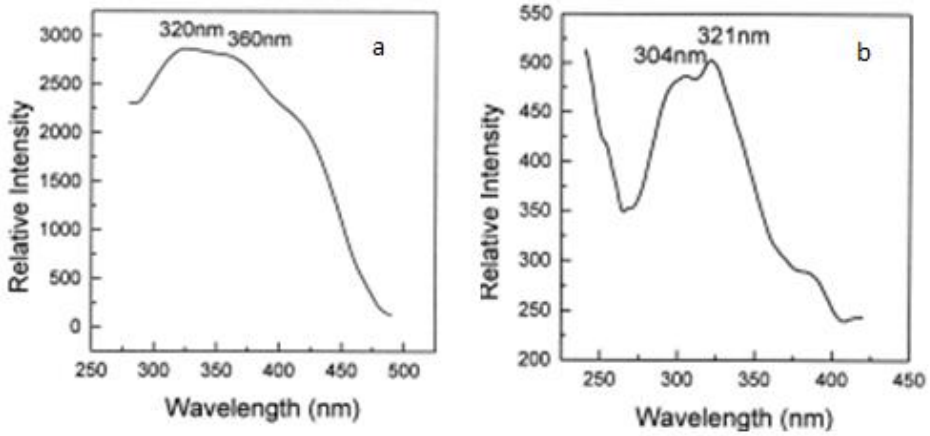

Figure 2.14 : Excitation spectra of a) solid-1380, b) gel-1380 [45].

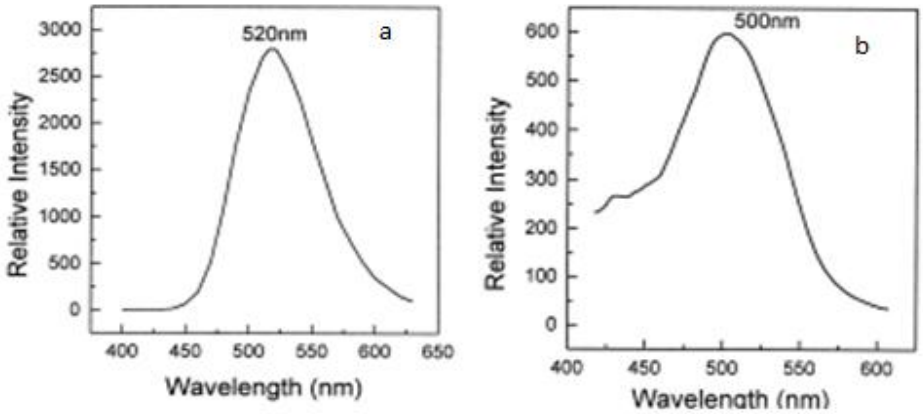

Figure 2.15 : Emission spectra of a) solid-1380, b) gel-1380 [45].

Luminescence and long after glow mechanism of nano $SrAl_2O_4$: Eu, Dy is associated with surface energy and crystal filed effect. Nanosize grains have higher surface

energy than micrometer sized grains which results in the distortion of atom structure and the change of the crystal field around Eu^{2+}. As mentioned above, although the 4f electron of Eu^{2+} is not sensitive to lattice environment, the 5d electrons may be influenced strongly. Consequently, the mixed states of 4f, 5d will be split by the crystal field, as a result, some jumps which are not allowed in micron $SrAl_2O_4$:Eu^{2+}, Dy^{3+}, can take effects in nano $SrAl_2O_4$:Eu^{2+}, $Dy^{3+}$and thus lead to the blue shift occurrence in the excitation and emission spectra. Figure2.16 shows the decay curve of nano and micron $SrAl_2O_4$: Eu, Dy. The luminescent intensity of nano grade is much less than that of the micron grade. This also can be attributed to the surface energy. The surface energy level is much deeper than the trap level of Dy and then can attract more vacancies than Dy, which results decreasing in initial luminescent intensity.

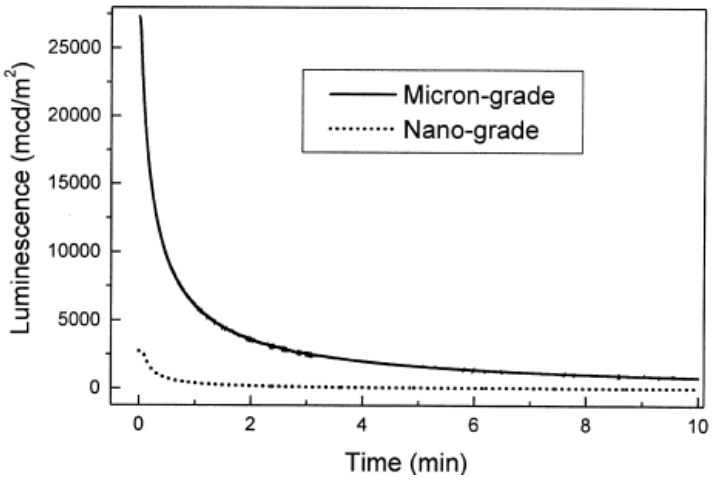

Figure 2.16 : Decay curves of nano and micron $SrAl_2O_4$: Eu, Dy [45].

Peng and Yang et al. [20] also studied the size dependency of phosphorescent characteristic of $SrAl_2O_4$: Eu^{2+}, Dy^{3+} phosphors. They prepared the materials by solution-combustion and solid state reaction methods. According to them, the sintering temperature of the nanometer phosphors decreases by about 400°C due to the high activity of nanometer powder and the uniform components comparing with the phosphors prepared by the solid-state reaction method. They also observed the blue shifts in emission and excitation spectra, and more rapidly decay than solid state samples. They associated these results with follow features of the phosphor nanoparticles:

- Quantum size effect which increased the kinetic energy of the electrons and resulted in a larger band gap, thus, needing higher energy to excite the luminescent powders,
- Crystal field effect which may cause splitting the mixed states of 4f, 5d and lead to the blue shift of its emission peak,
- Rate of hole mobility which has effect on determining the retraping probability, low rate of hole mobility and electron-hole recombination will increase retraping probability and further slow down the decay process,
- Structure defects which are serving as trap level and amount of defects are decreased due to easily and completely crystallization of phosphor nanoparticles during heat treatment process. Additionally, a lot of defects are dispersed on the surface of phosphors because of the high surface area of the nanoparticles, and which may result in relatively less amount of luminescent center Eu^{2+} in the $SrAl_2O_4$ lattice available for the direct radiation.

3. EXPERIMENT

In this study, it is aimed to synthesize $SrAl_2O_4$ based nanocrystalline phosphors and to investigate co-dopant effect of some of transition metals which are Fe, Ni, Co and Y on strontium aluminate phosphor activated with Eu^{2+} and Dy^{3+}. Also, size dependency of phosphorescence and structure properties are studied by synthesizing these phosphors with different methods, conventional solid state, modified sol-gel, and solution-combustion.

3.1 Chemicals and Procedure

In the experimental study, strontium nitrate $Sr(NO_3)_2$, strontium carbonate ($SrCO_3$), aluminum nitrate nonahydrate ($Al(NO_3)_3.9H_2O$), aluminum oxide (Al_2O_3), cobalt(II) nitrate hexahydrate ($Co(NO_3)_2.6H_2O$), iron(III) nitrate nonahydrate ($Fe(NO_3)_3.9H_2O$), nickel(II) nitrate hexahydrate ($Ni(NO_3)_2.6H_2O$), yttrium(III) nitrate hexahydrate ($Y(NO_3)_3.6H_2O$), europium(III) oxide (Eu_2O_3), dysprosium(III) oxide (Dy_2O_3), citric acid monohydrate ($C_6H_8O_7.H_2O$), boric acid (H_3BO_3) and urea (CH_4N_2O) are used as raw materials with high purity (99,99) (table 3.1). Samples were prepared with different co-doping composition of transition metals and yttrium in strontium aluminate host matrix material ($Sr_{0,92-X}M_XAl_2O_4$: $Eu_{0,02}$, $Dy_{0,06}$; M:Fe, Ni, Co and Y; X=0,005 and 0,01) to observe the effect of composition on phosphorescent characteristics and structure. Generally, amounts of raw materials are calculated to product 0,025 mol samples.

In solid state reaction method, only one composition ($Sr_{0,92}Al_2O_4$: $Eu_{0,02}$, $Dy_{0,06}$) are synthesized as reference sample. In this method, firstly calculated amount of raw materials were weighed with precision balance (0.0001 g. precision), then placed into the crucible with zirconia balls and sufficient amount of ethanol. The crucible was placed in planetary ball mill to ground the raw materials for 6 hours. Then, in order to remove ethanol, mixture was put into oven at 115°C for 24 hours. In order to remove residual organic compounds, obtained powders were calcined at 800°C for 6 hours. Then, samples were sintered at 1300°C in %5 H_2/N_2 reductive atmosphere for

one and two hours to determine the effective reaction time. XRD, SEM and spectrophotometer were used to investigate the structural, morphological and optical analysis, respectively. In figure 3.1, the flow chart of sol-gel and combustion methods are given.

Table 3.1 : Used raw materials in different synthesis methods.

Raw Materials	Molar Weight (g/mol)	Solid State Reaction	Sol-Gel	Combustion
$Sr(NO_3)_2$	211,63		X	X
$SrCO_3$	147,63	X		
$Al(NO_3)_3.9H_2O$	375,13		X	X
Al_2O_3	102	X		
$Co(NO_3)_2.6H_2O$	291,04		X	X
$Fe(NO_3)_3.9H_2O$	404		X	X
$Ni(NO_3)_2.6H_2O$	290,79		X	X
$Y(NO_3)_3.6H_2O$	383,01		X	X
Eu_2O_3	351,93	X	X	X
Dy_2O_3	373	X	X	X
$C_6H_8O_7.H_2O$	210,14		X	
H_3BO_3	61,83	X	X	X
CH_4N_2O	60,07			X

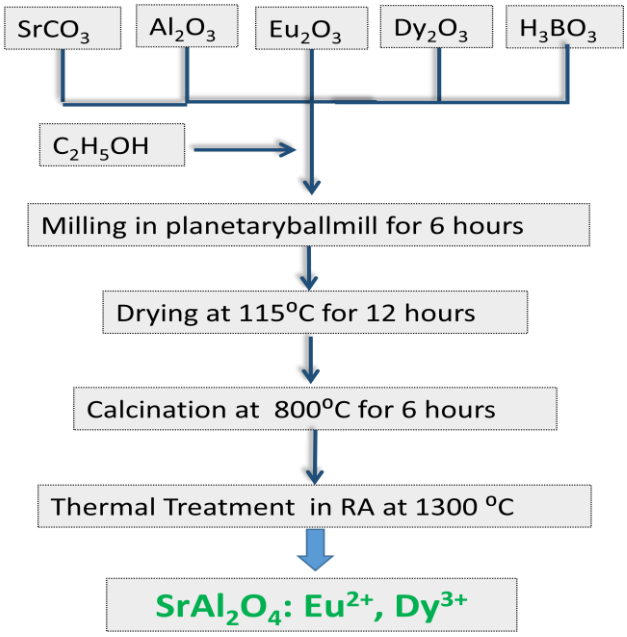

Figure 3.1 : Flow Chart of the solid state synthesis method.

In sol-gel reaction method, calculated samples were weighed with precision balance firstly. Nitrate based compounds and boric acid were dissolved with deionized distilled water (DDW) in a beaker. On the other hand, in order to obtain nitrate forms of oxide based compounds, they were dissolved with concentrated nitric acid. All solution stirred with magnetic stirrer (WiseStir MSH-20A) at 100°C until the solutions became homogeneous and transparent and then two solutions were combined in a 100 ml beaker. After complete dissolution, citric acid was added to the system as chelating agent to achieve a 2:1 ratio of CA to total metal ions in the solution. [1,2]. By keeping the solution at 100°C for 2-3 hours under constant stirring, the solution becomes viscous. After the sol was dried at 200°C for 12 h, brown dried-gels were obtained. The dried-gels were calcined at 800°C in air atmosphere for 6 h to remove the residual carbon. Finally, the calcined powders were sintered up to 1300°C for 1 h in reducing atmosphere.

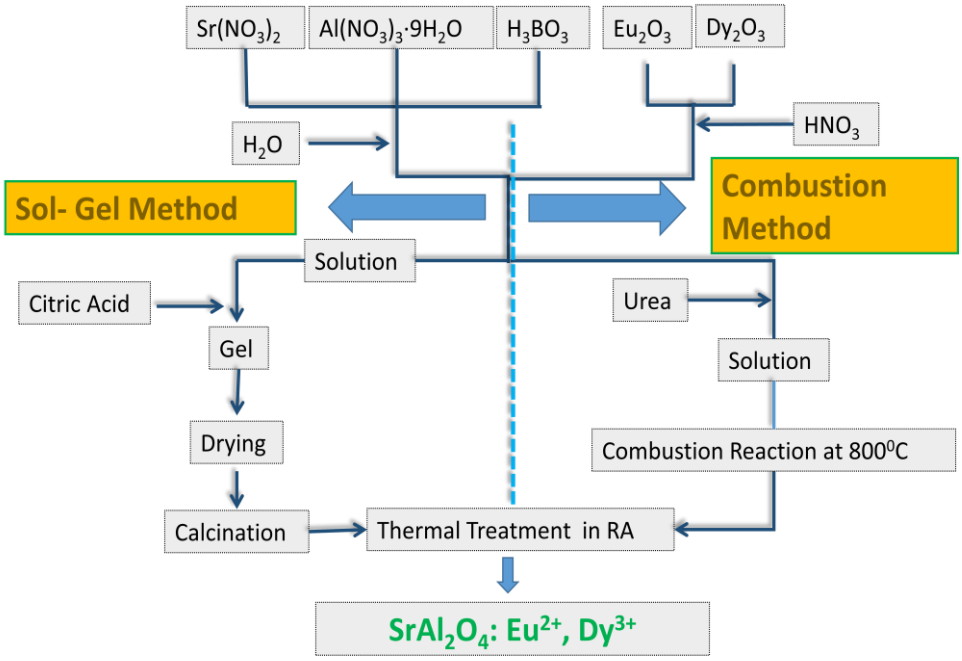

Figure 3.2 : Flow Chart of the sol-gel and combustion methods.

In solution-combustion method, raw materials were weighted according to the composition. One solution was prepared by dissolving nitrate based compounds into DDW, and another one was obtained by dissolving oxide based compounds in concentrated nitric acid. Two solutions were then mixed. The following step was to add urea into the aqueous solution. The amount of urea in mole was 1.5 times of theoretical value. The solution was kept at 100°C under constant stirring to become

homogeneous and transparent. Then the solution was poured into a crucible, which was transferred to a muffle furnace preheated at 600°C and 800°C. Initially, the solution boiled, followed by decomposition with the evolution of large amounts of gases (oxides of carbon and nitrogen). Then, spontaneous ignition occurred and underwent combustion with enormous swellings occurring. The entire combustion process would last a few minutes. In figure 3.2, the flow chart of sol-gel and combustion methods are given.

3.2 Characterization tools

3.2.1 XRD characterization

X-ray diffraction (XRD) studies of the samples was carried out using a Philips™ PW 3710 X-Ray diffractometer with Cu-K_α radiation (λ=0.15418 nm), V=40 kV and I=40 mA in the 2θ range of 10- 90°. Phases in structure were determined by comparing the peak positions and intensity with the JCPDS (Joint Committee on Powder Diffraction Standards) data file.

Figure 3.3 : Philips™ PW 3710 X-Ray diffractometer.

3.2.2 SEM characterization

The morphology and the size of phosphors powders were observed using scanning electron microscope (JEOL™ JSM 5410 SEM). Because of all samples were insulator, all samples were coated with platinum in order to achieve conductive surfaces before SEM measurements.

Figure 3.4 : JEOL^{TM} JSM 5410 Scanning Electron Microscope.

3.2.3 Optical characterization

Measurements of emission and excitation intensity and phosphorescence decay time of the samples were carried out using Varian Fluorescence Spectrometer. Setup parameters were set according to the highest emission intensity sample and the results were obtained based on the setup parameters. Samples were excited in the wavelength range 300 to 500 nm and emission behaviors were investigated in the wavelength range 400 to 650 nm. Decay lifetime analyses were made in 5 millisecond time interval after excitation 0.1 millisecond for all samples. Additionally, in order to analyze the afterglow decay time characteristics of the samples, decay time curves are fitted to equation 3.1

$$y = y0 + A1 * e^{-\frac{x}{\tau 1}} + A2 * e^{-\frac{x}{\tau 2}} \quad \textbf{(3.1)}$$

where, y is luminescence intensity at the time of any x, A_1 and A_2 is constants, τ_1 and τ_2 are the exponential afterglow times.

Figure 3.5 : VARIAN^{TM} Fluorescence Spectrophotometer.

4. RESULTS AND DISCUSSIONS

As mentioned above, the production of strontium aluminate based phosphorescence materials is the aim of this study. So, before the production, it is required to optimize the synthesis conditions. In order to optimize the synthesizing conditions, various experiments were done. One of them is determining the effective time duration for thermal treatment of $SrAl_2O_4$: Eu^{2+}, Dy^{3+} and the other is determining the effective ignition temperature for $SrAl_2O_4$: $Eu^{2+,}$ Dy^{3+} based phosphors synthesized with combustion method. After determination of optimum synthesis conditions, phosphorescence samples were produced and characterized. Results from the experimental studies are described as in the following:

1. The effect of synthesis method on microstructural and luminescence properties of un-doped $SrAl_2O_4$: Eu^{2+}, Dy^{3+} phosphors
2. The effects of dopant type and concentration on microstructural and luminescence properties of $SrAl_2O_4$: Eu^{2+}, Dy^{3+} phosphors

4.1 The Effect of Synthesis Method on Luminescence and Microstructural Properties of Un-Doped $Sral_2o_4$: Eu^{2+}, Dy^{3+} Phosphors

According to the literature, the best luminescence properties are obtained when only monoclinic $SrAl_2O_4$ phase forms in the structure. So, it is tried to obtain only monoclinic $SrAl_2O_4$ phase in the structure while determining the optimum conditions. In order to determine the effective reaction time, europium and dysprosium doped strontium aluminate phosphors were synthesized with solid state reaction method for 1, 3 and 6 hours.

It is reported that obtaining monoclinic $SrAl_2O_4$ phase in the structure is possible when temperature is above 1250°C.Therefore, we selected 1300°C as reaction temperature which is mostly used as temperature to produce these phosphors in the literature. We thought that higher temperatures than 1300°C may cause partial melting problems in the structure. In table 4.1, used raw materials are given.

Additionally, phosphor samples were synthesized with combustion methods using two ignition temperature (600 and 800°C which are below and above temperature of monoclinic to hexagonal phase transition temperature (650°C)) in order to determine the effective ignition temperature for combustion synthesis. Used raw materials for the synthesis of $SrAl_2O_4:Eu^{2+}$, Dy^{3+} combustion samples are shown in table 4.2.

Table 4.1 : Used raw materials for synthesizing 0,024 mol $Sr_{0,92}Al_2O_4$: $Eu_{0,02}$ $Dy_{0,06}$ with solid state reaction.

Precursor Materials	Amounts (gr)
$Sr(CO)_3$	3,2129
Al_2O_3	2,4129
Eu_2O_3	0,0832
Dy_2O_3	0,2647
H_3BO_3	0,1225

After determining the optimum conditions, phosphor samples were synthesized with solid state, sol-gel and solution-combustion methods and then characterized. In this thesis sol-gel (Pechini) and solution-combustion methods were used to produce nano grain sized phosphor particles. Also solid state reaction method was used to be able to compare our nanophosphor in the way of structural and optical properties.

Table 4.2 : Used raw materials to synthesized 0,023 mol $SrAl_2O_4:Eu^{2+}$, Dy^{3+} (5 g) by combustion method.

Precursor Materials	Amounts (gr)
$Sr(NO_3)_2$	4,3768
$Al(NO_3)_3.9H_2O$	16,8658
EU_2O_3	0,07911
Dy_2O_3	0,2515
H_3BO_3	0,1187
CH_4N_2O	13,51048787

4.1.1 X-ray characterization

X-ray diffractometer analysis was carried out to examine existing phases in the structure after thermal treatment. XRD results of $SrAl_2O_4$: Eu^{2+}, Dy^{3+} phosphors synthesized with solid state method annealed at 1300°C in H_2/N_2 reducing atmosphere for 1,3 and 6 h are given in figure 4.1.

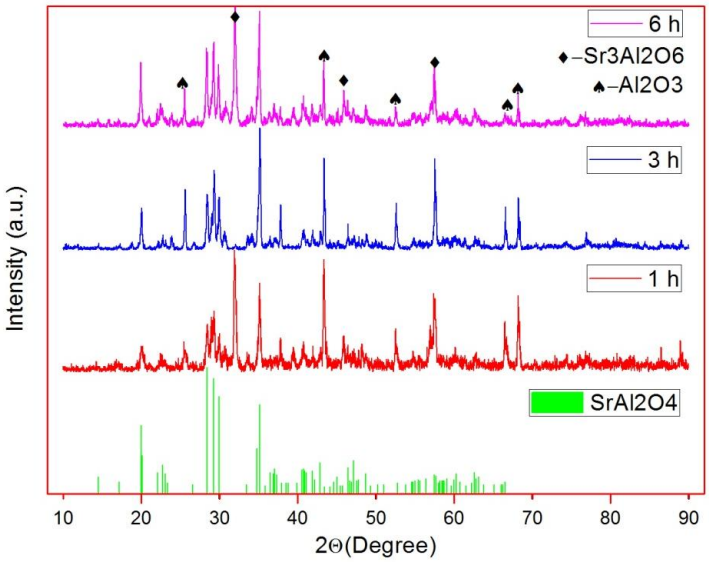

Figure 4.1 : XRD patterns of $SrAl_2O_4$: Eu^{2+}, Dy^{3+} phosphors synthesized with solid state method annealed in H_2/N_2 RA for 1, 3 and 6 hours.

According to figure 4.1, there are three phases, monoclinic $SrAl_2O_4$ (34-0379), cubic $Sr_3Al_2O_6$ (24-1187), and rhombohedral Al_2O_3 (10-0173), in 1 and 6 hours annealed samples. It is possible for us to speculate about the mechanism of formation of $SrAl_2O_4$in solid state reaction. It can be summarized as follows:

1. The precursors may be segregated to $SrCO_3$and alumina.

2. $SrCO_3$ reacted with alumina to form intermediate phase $Sr_3Al_2O_6$,

$$Al_2O_3 + 3SrCO_3 \rightarrow Sr_3Al_2O_6 + 3CO_2 \quad \textbf{(4.1)}$$

3. $SrAl_2O_4$formed by the reaction:

$$2Sr_3Al_2O_6 + Al_2O_3 \rightarrow 3SrAl_2O_4 \quad \textbf{(4.2)}$$

For 3 hours annealed sample, monoclinic $SrAl_2O_4$ and Al_2O_3 are seen in the pattern. In this study, monoclinic $SrAl_2O_4$ is only desired phase in the structure. So 3 hour is selected as effective annealing time due to there is no $Sr_3Al_2O_6$ phase in the structure. Additionally, 3 hour is chosen as reaction time duration in the most of reports.

The Scherrer formula (4.3) is used to calculate the crystalline size of the monoclinic $SrAl_2O_4$.

$$\tau = \frac{K\lambda}{\beta \cos\theta} \quad \textbf{(4.3)}$$

where τ is the mean size of the ordered (crystalline) domains, K is a dimensionless shape factor (0.9), λ is the X-ray wavelength (0.15418 nm), θ is the Bragg angle and β is the line broadening at half the maximum intensity. Before the application of the Scherrer formula, contributions such as dislocations, stacking faults, twinning, micro stresses, grain boundaries and sub-boundaries, which cause the peak broadening must be eliminated. So, before applying Scherrer formula, the Kalpha1-Kalpha2 interaction is stripped and the background of the patterns was eliminated. According to 220 peak of monoclinic $SrAl_2O_4$, 28.53, 34.23 and 42.8 are the calculated crystalline size of the 1, 3 and 6 hours annealed samples, respectively.

In combustion case, it is reported that the effective ignition temperature for combustion synthesis is 600°C. However, we observed better results in XRD and optical measurements for 800°C sample. XRD patterns of synthesized particles before (BA) and after annealing (AA) in reductive atmosphere are given in figure 4.2.

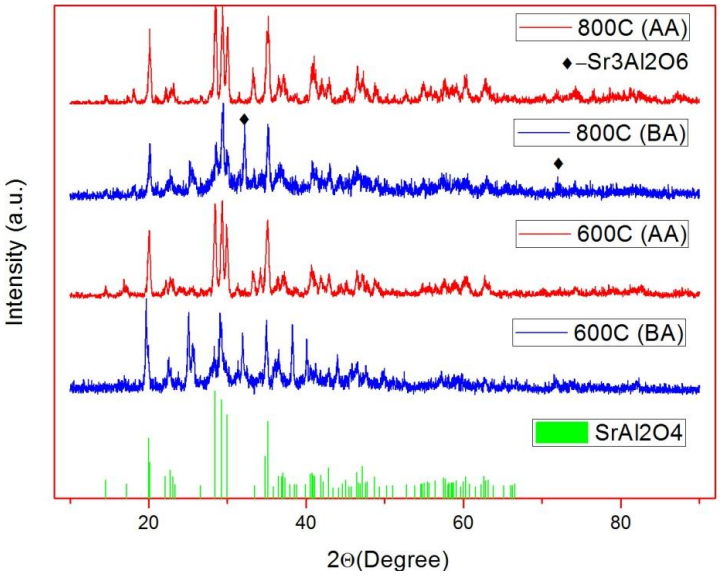

Figure 4.2 : XRD patterns of $SrAl_2O_4$: Eu^{2+}, Dy^{3+} phosphors synthesized with combustion method ignited at 600 and 800°C before (BA) and after annealing (AA) at 1300°C in RA.

According to the patterns, in before annealing case, there are $SrAl_2O_4$ phase together with impurity phase, $Sr_3Al_2O_6$, which affect the luminescence properties in negative way. Additionally, crystallinity of the sample ignited at 800°C is better than 600°C one. After annealing, there are no impurity phases in the structure of both samples. Ignited at 800°C sample also includes more intense peak of monoclinic $SrAl_2O_4$

phase than ignited at 600°C one. So selecting 800°C as ignition temperature is more reasonable.

After determining the optimum synthesis conditions, phosphor samples were synthesized and characterized. In figure 4.3, XRD patterns of $SrAl_2O_4$: Eu^{2+}, Dy^{3+} phosphor synthesized with a) solid state, b) sol-gel (Pechini) and c) solution-combustion methods annealed in H_2/N_2 reducing atmosphere for 3 h are shown. According to the figure, there is an impurity phase, Al_2O_3, near the $SrAl_2O_4$ main phase in XRD pattern of solid state sample. In the case of combustion and Pechini, there are only monoclinic $SrAl_2O_4$ peaks in the XRD patterns. Additionally, it is observed that the combustion sample shows higher crystallinity and have more intense peaks than the others. These results confirm that solution based methods provide a satisfactory condition for the formation of single phase $SrAl_2O_4$.

Crystalline sizes of the samples are calculated using equation 4.3. According to results 21.4, 34.26 and 42.8 are the calculated crystalline sizes for combustion, Pechini and solid state samples, respectively.

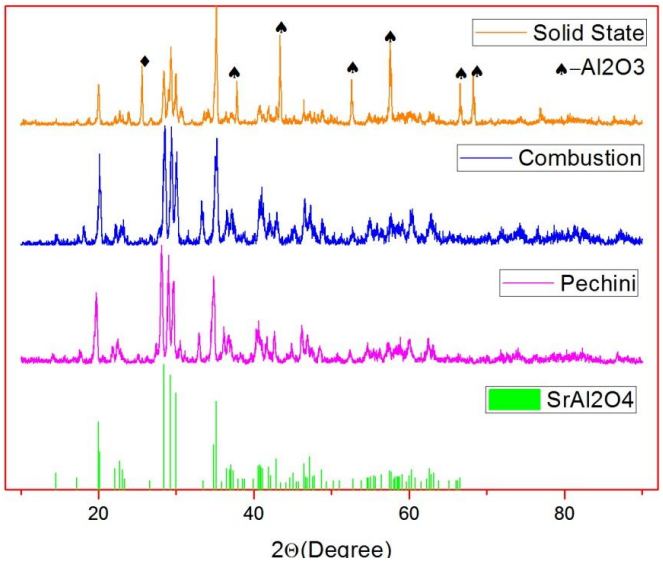

Figure 4.3: XRD patterns of $SrAl_2O_4$:Eu^{2+}, Dy^{3+} phosphor synthesized with a) solid state, b) Sol-gel (Pechini) and c) Sol-combustion methods annealed in H_2/N_2 RA for 3 h.

It was thought that the presence of higher intensity peaks of $SrAl_2O_4$ in combustion samples is a result of obtaining nano-sized particles. It is known that particles with finer size have higher surface area which means higher reactivity. So, chemical reactions can occur more easily. Additionally, homogeneity of precursor materials has also positive effect on crystallization. In combustion synthesis precursor

materials can be mixed at almost molecular level and have the best homogeneity among the others. Additionally, obtaining $SrAl_2O_4$ powders at low ignition temperature (800°C) in a very short time interval (3-5 min) and absence of any calcination treatment gives finer size powders. These conditions provide higher possibility to obtain only monoclinic $SrAl_2O_4$ phase in the structure than others.

In solid state reactions, particle size of precursors can be reduced maximum micrometer range with mechanical milling and after milling particles can be precipitate non-homogeneously due to their density differences. In Pechini method, pH of solution is very critic to obtain homogeneous precursor mixture. Additionally, this process has calcination steps which starts the crystallization in unwanted way and causes grain size growth. So, we obtain less $SrAl_2O_4$ phase in the structure of Pechini and solid state samples than combustion one.

4.1.2 SEM characterization

SEM analysis was carried out to view the sintered powder morphologies. In figure 4.4, SEM micrograph of phosphor samples synthesized with a) solid state, b) solution-combustion and c) sol-gel (Pechini) methods (which are annealed in RA at 1300°C for 3 h) are shown. We can see that the whole consists of highly sintered structure. Sharp edges are as a result of grinding process after sintering. In the case of combustion, in the structure, partial melting region is observed which an evidence of that combustion sample can easily and quickly sintered than others due to having finer particle size.

4.1.3 Optical characterization

UV-Visible spectrophotometer was used to determine emission and excitation characteristics of these phosphors. For determination of excitation and emission spectrum, measurements between λ=300-450 nm and λ=400-650 nm were carried out, respectively. Also afterglow decay characteristics of the samples were measured for 500msec time intervals after excitation of 0.1 msec UV radiation.

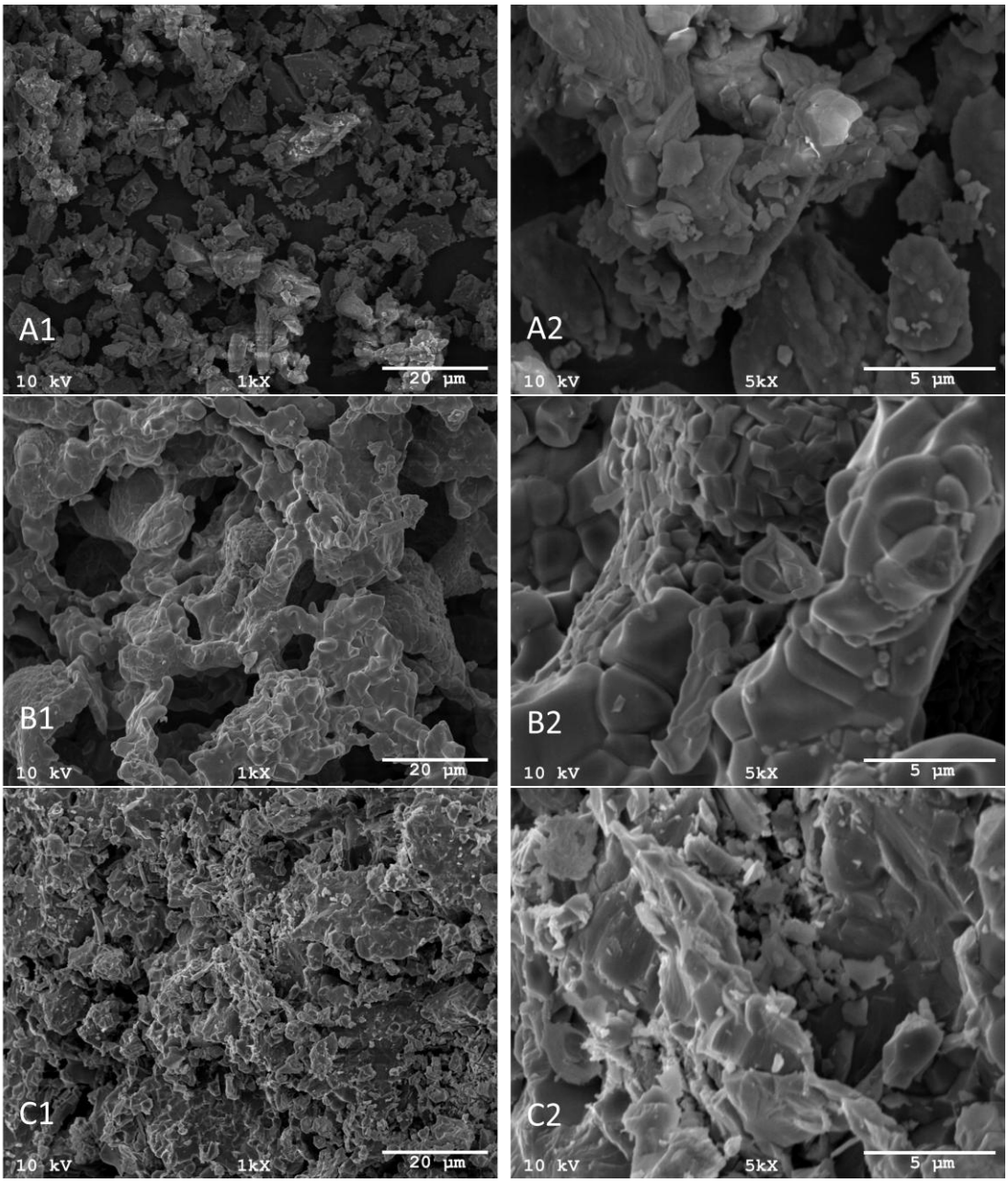

Figure 4.4 : 1000X and 5000X magnified SEM micrographs of phosphor samples synthesized with a) solid state, b) Pechini and c) combustion methods.

In figure 4.5, emission and excitation spectrums of $SrAl_2O_4$: Eu^{2+}, Dy^{3+} phosphors annealed in H_2/N_2reducing atmosphere for 1, 3 and 6 h are shown. According to figure, all samples have the same shape of emission and excitation spectrums. Additionally, all of them have broad excitation spectrums which also include a part of visible spectrum. But peak intensities of both spectrums for 3 hour annealed sample are relatively higher than the 1 hour annealed one and lower than 6 hours annealed one. From 300 to 450 nm, the excitation spectrum of the phosphors shows two wide bands with their peaks at about 335 and 360 nm, respectively. These can be

attributed to the crystal field splitting of the Eu^{2+} d-orbital. In excitation spectra, peak at 370 nm is originating from the instrument and peak at 417 is due to specimen holder band.

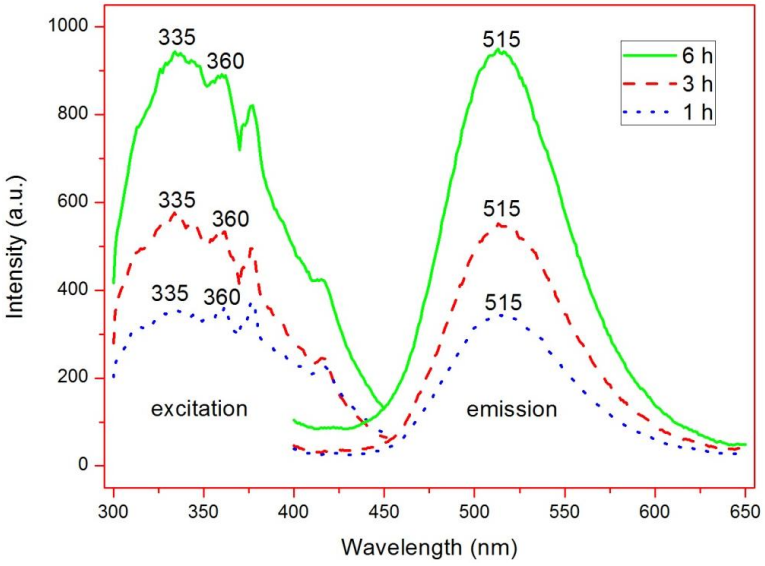

Figure 4.5 : Emission and excitation spectrums of $SrAl_2O_4$: Eu^{2+}, Dy^{3+} phosphors synthesized with solid state method annealed in RA for 1, 3 and 6 h.

The emission spectrum after excitation at 335 nm includes a broad band peaked at 515 nm which is the phosphorescence of Eu^{2+} ions in $SrAl_2O_4$ luminescence result from transitions between the $4f^6 5d^1$and $4f^7$ electron configurations. Although the 4f electrons of Eu^{2+} are not sensitive to crystal lattice environment due to the shielding function of outer shell, the 5d electrons can easily coupled with crystal lattice, thus the 4f-5d hybridization state can be split by the influence of crystal field and coupled strongly with crystal lattice phonon, which leads to a broad band emission.

On the other hand, afterglow decay result of 3 hour annealed sample is also higher than 1 and lower than 6 hours annealed sample (figure 4.6). In table 4.2, afterglow decay parameters of $SrAl_2O_4$: Eu^{2+}, Dy^{3+} phosphor synthesized with solid state method is given. The decay characteristics of $SrAl_2O_4$: Eu^{2+}, Dy^{3+} phosphor indicates that the decay process contains a rapid-decaying and a slow-decaying process. Initial rapid decaying is attributed to relaxation of excited electrons of Eu^{2+} ions and following slow decaying is attributed to thermally releasing of trapped electrons in Dy^{3+} sites and relaxation to ground state of Eu^{2+}.

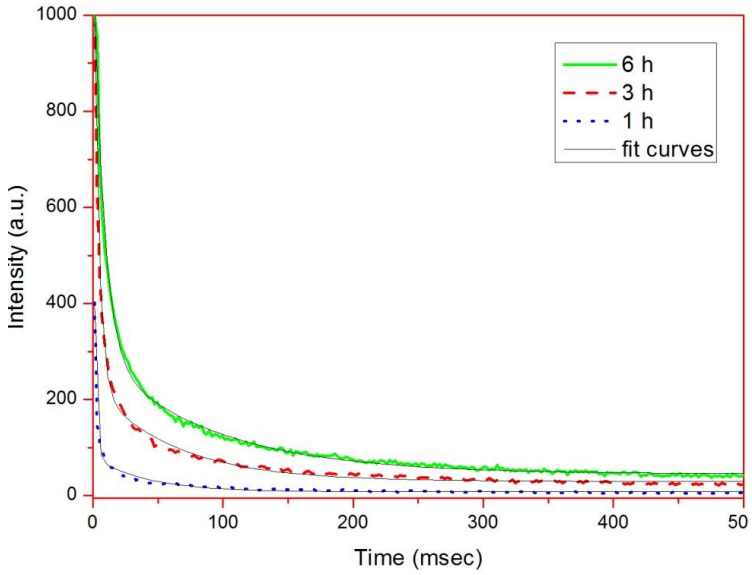

Figure 4.6 : Afterglow decay curves of of $SrAl_2O_4$: Eu^{2+}, Dy^{3+} phosphors synth. with solid state method annealed in H_2/N_2RA for 1, 3 and 6 h.

Table 4.3 : Afterglow decay parameters of $SrAl_2O_4$: Eu^{2+}, Dy^{3+} phosphor synth. with solid state method.

Samples	**y_0**	**A_1**	**A_2**	**τ_1**	**τ_2**
1 h	7,96	642,51	73,10	1,576	41,05
3 h	29,93	199,27	1009,24	61,51	3,80
6 h	45,36	253,42	842,93	88,5	7,95

Producing phosphor particles with nano grain size is aimed in this thesis. It is thought that 1 h as annealing time inhibits particle size growth to obtain particles with nano grains. Additionally, particle size of synthesized phosphors with Pechini and combustion methods are finer than solid state samples which means more reactivity due to higher surface area. So annealing for 1 h at 1300°C in H_2/N_2 atmosphere was considered enough to reduce Eu^{3+} to Eu^{2+} and obtain monoclinic $SrAl_2O_4$ in the structure in the sol-gel and combustion synthesis methods. Experimental results also verified our approximation (figure 5.1).

In order to examine afterglow decay characteristics of the $SrAl_2O_4$ based phosphors, sample was exposed to UV radiation with different number of flushing. According to figure, it can be seen that initial intensity and luminescence lifetime increased while number of flushing is increasing. But there is no change in decay characteristics while number of flushing is increasing. There is only two components in the decay curves, first is rapid decaying and the other is slow decaying in all curves which is a result of phosphorescence mechanism is independent from exposure time. So, it is reasonable to fit the curves using equation 3.1 which includes two exponential decay

parameters. Obtained decay curves and decay parameters were given in figure 4.7 and table 4.4, respectively.

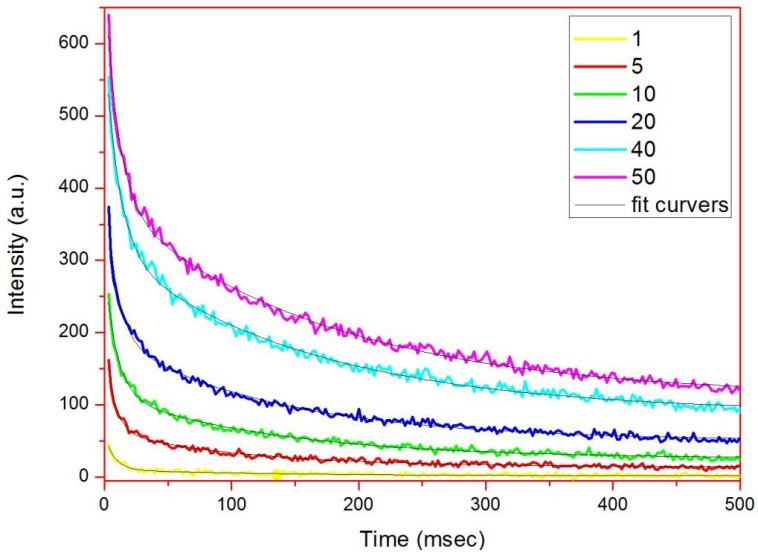

Figure 4.7 : Effect of number of flashing on the afterglow decay curves of 3 hour annealed solid state sample.

Table.4.4 : Effect of number of flushing on the afterglow decay parameters of $SrAl_2O_4$: Eu^{2+}, Dy^{3+} phosphor synthesized with solid state method.

No of flashes	**1**	**5**	**10**	**20**	**40**	**50**
$\mathbf{y_0}$	1,96	14,21	25,75	50,81	89,55	111,44
$\mathbf{A_1}$	8,83	51,04	181,00	224,28	286,99	310,75
$\boldsymbol{\tau_1}$	123,85	104,94	9,07	8,88	10,96	10,35
$\mathbf{A_2}$	49,09	146,92	90,32	145,76	228,61	273,96
$\boldsymbol{\tau_2}$	7,38	6,53	132,14	130,13	156,38	169,18

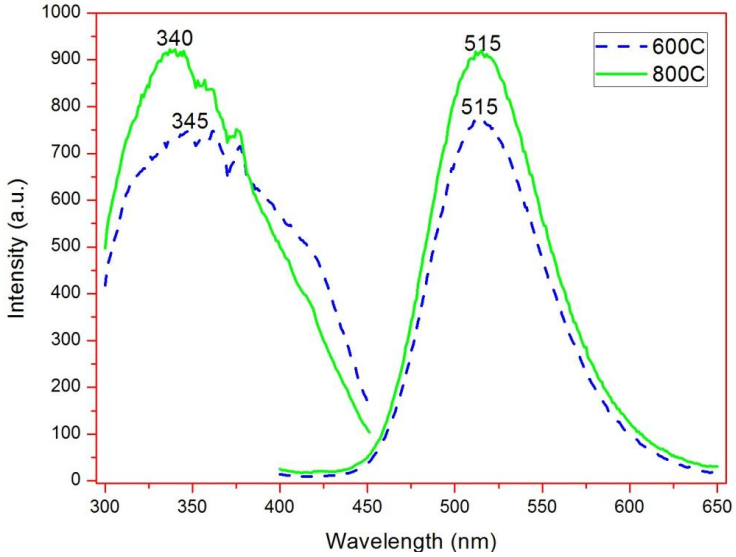

Figure 4.8 : Emission and excitation spectrums of $SrAl_2O_4$: $Eu^{2+,}$ Dy^{3+} phosphors synthesized with combustion method annealed in H_2/N_2RA for 3 h.

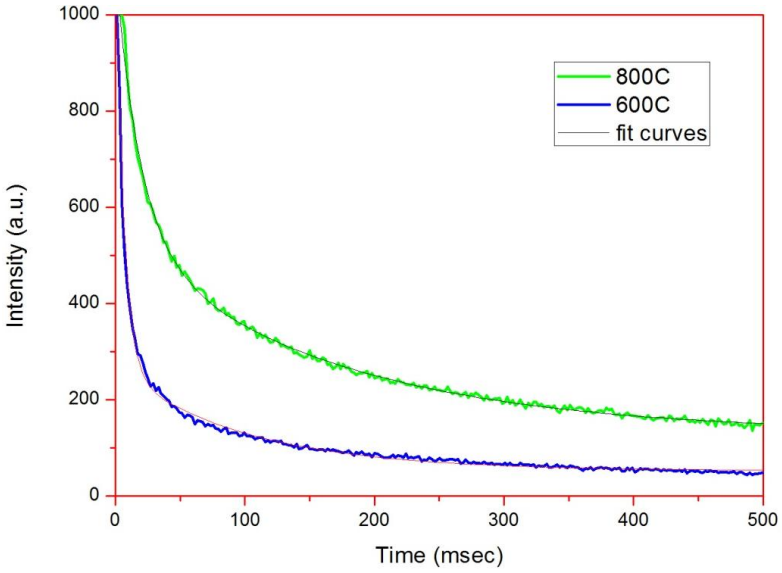

Figure. 4.9 : Afterglow decay curve of $SrAl_2O_4$: Eu^{2+}, Dy^{3+} phosphors synth. with combustion method annealed in H_2/N_2 reducing atmosphere for 3 h.

Emission / excitation spectrums and afterglow decay curves for the combustion samples are given in figure 4.8 and 4.9, respectively. In the literature, although there are a lot of reports about obtaining emission from combustion samples without any annealing in reducing atmosphere, any emission peak is not observed before annealing at 1300°C in reductive atmosphere. According to figure 4.7, both samples have nearly same shape of emission and excitation curve, but 800°C ignited sample shows more intense emission and excitation spectra which are peaked at 515 and 340 nm, respectively. Also, sample ignited at 800°C has longer afterglow lifetime. So selecting 800°C as ignition temperature for combustion synthesis is reasonable. Decay time parameters are obtained by fitting curves using equation 3.1 and given in table 4.5.

Table 4.5 : Afterglow decay parameters of $SrAl_2O_4$: Eu^{2+}, Dy^{3+} phosphor synthesized with Combustion method ignited at 800 and 600C.

Samples	**y_0**	**A_1**	**A_2**	**τ_1**	**τ_2**
800°C	52,21	884,09	212,27	6,22	100,21
600°C	131,17	402,19	558,78	164,49	19,25

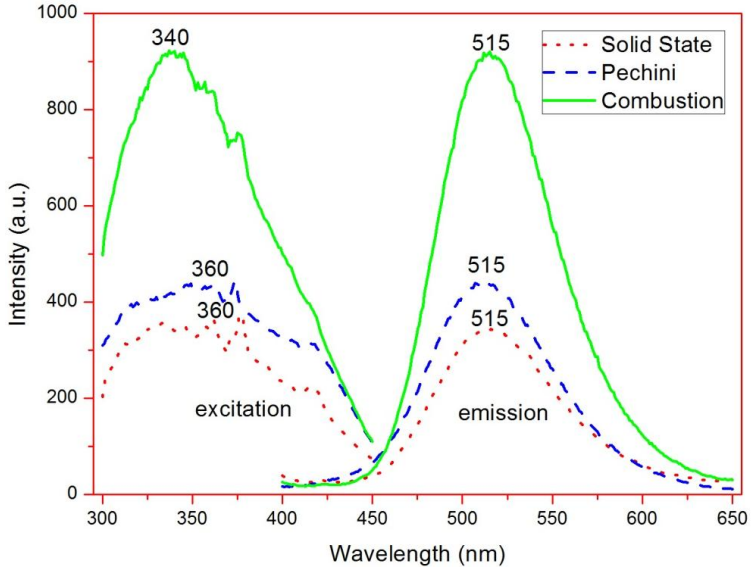

Figure 4.10 : Emission and excitation spectrums of $SrAl_2O_4$: Eu^{2+}, Dy^{3+} phosphor synthesized with a) solid state, b) Pechini and c) combustion methods annealed in H_2/N_2 RA for 3 h.

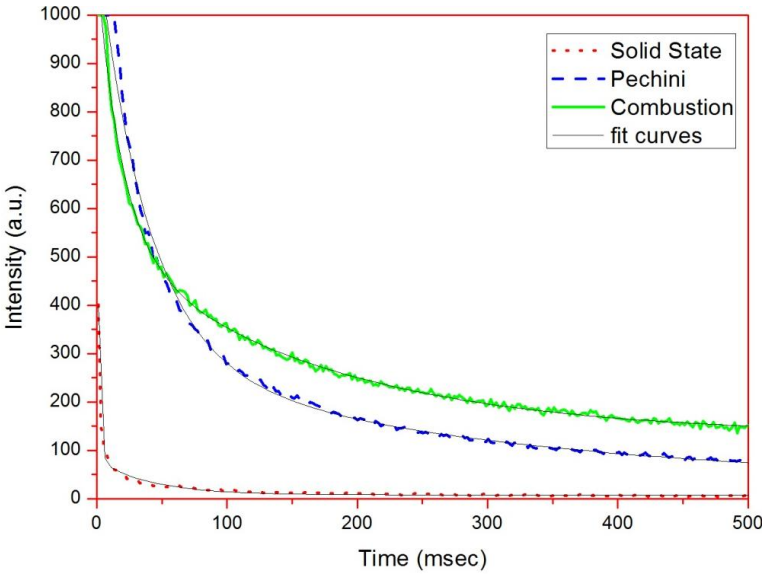

Figure 4.11 : Afterglow decay curves of $SrAl_2O_4$: Eu^{2+}, Dy^{3+} phosphor synthesized with a) solid state, b) Pechini and c) combustion methods annealed in H_2/N_2 RA for 3 h.

In figure 4.10 and 4.11, emission / excitation and afterglow decay spectrums of $SrAl_2O_4$: Eu^{2+}, Dy^{3+} phosphor synthesized with solid state, Pechini and combustion methods are shown, respectively. Although emission wavelength is nearly same which is 515 nm and emission spectrums have the same shape for all samples, intensities of emission spectrums are different. The same results are almost observed in excitation spectrums of Pechini and solid state methods where maximum peaks are

located at 360 nm. Combustion sample has a nearly symmetric curve which is centered at 340 nm.

In both of the spectrums, combustion sample shows maximum intensity, then Pechini and solid state samples follow it, respectively. This result is also compatible with the literature. Monoclinic $SrAl_2O_4$ with the highest peak intensity was obtained in the structure of the combustion sample which optical results are the highest. When we look at afterglow spectrums combustion sample have the longest lifetime. According to equation 3.1, afterglow decay time parameters are shown in table 4.6.

Table 4.6 : Afterglow decay parameters of $SrAl_2O_4$: Eu^{2+}, Dy^{3+} phosphor synth. with solid state, Pechini and combustion methods.

Samples	y_0	A_1	A_2	τ_1	τ_2
Combustion	131,17	402,19	558,78	164,49	19,25
Pechini	31,51	265,57	851,81	275,00	38,54
S. State	7,96	642,51	73,10	1,57	41,05

4.2. Effect of Doped Elements on Luminescence and Microstructural Properties of $SrAl_2O_4$: Eu^{2+}, Dy^{3+} Phosphor Synthesized by Combustion and Pechini Methods

4.2.1 Effect of Co dopant

In order to investigate the effect of 0,5% and 1% Co as dopant material on $SrAl_2O_4$:Eu^{2+}, Dy^{3+} phosphor, samples were synthesized with Pechini and combustion methods using raw materials in table 4.7.

Table 4.7: Used raw materials for synthesizing of $Sr_{0,92-x}Co_xAl_2O_4$:Eu^{2+}, Dy^{3+} (x=0,005 and 0,01)

Precursor materials	Pechini		Combustion	
	0.5%	1%	0.5%	1%
$Sr(NO_3)_2$	4,5589	4,5123	4,5839	4,5620
$Co(NO_3)_2.6H_2O$	0,03425	0,0681	0,03444	0,0689
$Al(NO_3)_3.9H_2O$	17,6634	17,5792	17,7604	17,7725
EU_2O_3	0,0828	0,0824	0,0833	0,0833
Dy_2O_3	0,2634	0,2621	0,2648	0,2650
H_3BO_3	5,3094	5,3348	5,2804	5,2768
$C_6H_8O_7.H_2O$	29,684	29,5425		
CH_4N_2O			14,2271	14,2368

4.2.1.1 X-ray characterization

XRD patterns of 1% Co-doped $SrAl_2O_4:Eu^{2+}$, Dy^{3+} synthesized with Pechini and combustion methods are shown in figure 4.12. According to the figure, $SrAl_2O_4$ is main phase for both samples but Pechini sample shows more intense peak of $SrAl_2O_4$. So it can be said that addition of trace amounts of cobalt has no effect on the crystal structure of the Pechini sample. But it causes the formation of an impurity phase ($Sr_4Al_{14}O_{25}$-521876) in combustion case. Grain sizes of the samples are calculated using equation 4.3 and results for Pechini sample is 28,52 and for combustion one is 34,24 nm.

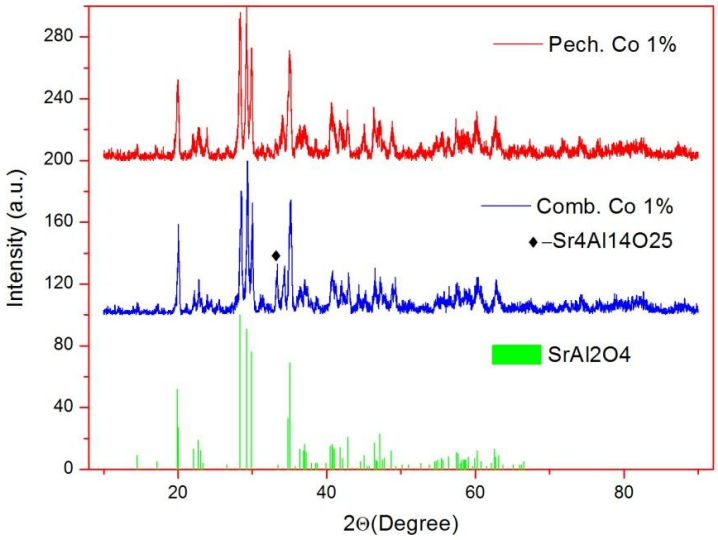

Figure 4.12 : XRD patterns of 1% Co-doped $SrAl_2O_4:Eu^{2+}$, Dy^{3+} synthesized with Pechini and combustion methods.

4.2.1.2 Optical characterization

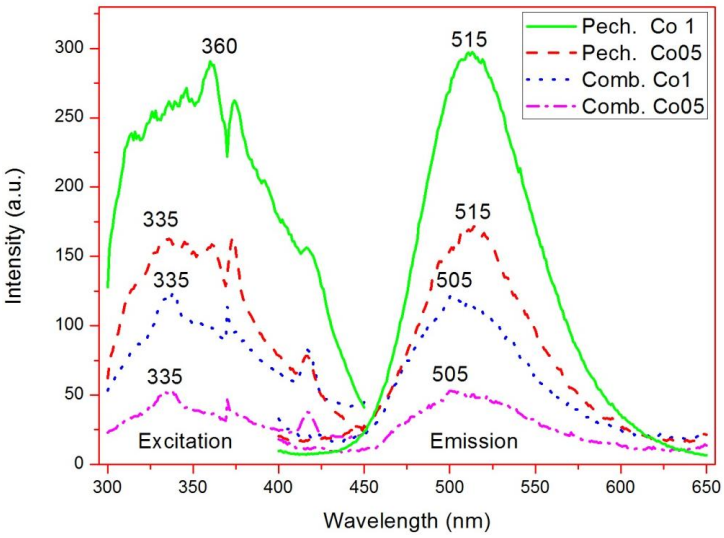

Figure 4.13 : Emission and excitation spectrums of Co-doped $SrAl_2O_4:Eu^{2+}$, Dy^{3+}synthesized with Pechini and combustion methods.

Emission and excitation spectrums of Co-doped $SrAl_2O_4:Eu^{2+}$, Dy^{3+} phosphor synthesized with Pechini and combustion methods are given in figure 4.13. According to the figure, 1% Co doped Pechini sample has maximum intensity in emission and excitation spectrums peaked at 515 and 360 nm, respectively. For 0,5 % Co doped Pechini sample, intensities of the spectrums are relatively low. Differences between excitation spectrums of 1and 0.5% doped samples are due to formation of different defects in the structure when dopant concentration increased. Different defects changes the crystal field near the Eu^{2+} ions so there will be different excitation level due to crystal field splitting. So, we can say that increasing dopant concentration causes different excited states in Pechini method. But having the same emission spectrum shows that transition from lowest excited level to ground level has same energy interval.

The situation is different for combustion samples. Doping concentration has an adverse effect on luminescence properties of combustion sample; increasing dopant concentration results decreasing luminescence properties. 1 and 0.5 % Co doped combustion samples have peaks at 505 and 335 nm in emission and excitation spectrums, respectively. Moreover, there is no difference between excitation spectrums of 1and 0.5 % doped samples in combustion case. Peak intensities for both of combustion samples are lower than Pechini samples. Additionally, according to peak points, we can see a blue shift in the both spectrums for combustion samples.

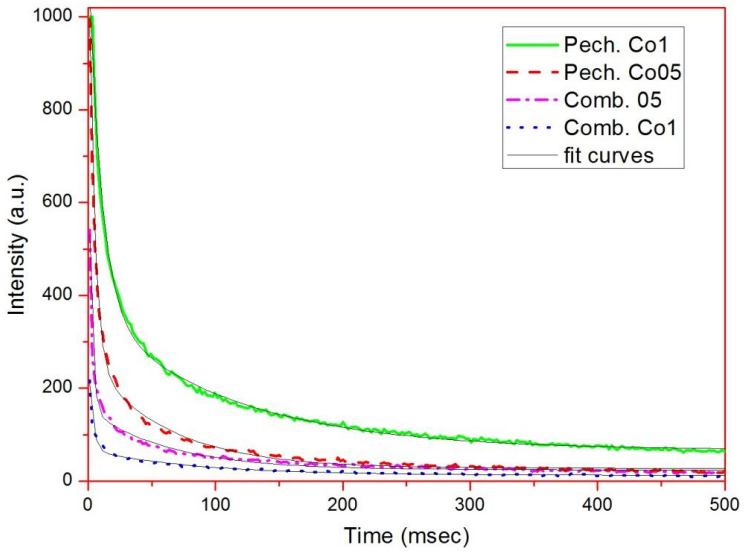

Figure 4.14 : Afterglow decay curves of Co-doped $SrAl_2O_4:Eu^{2+}$, Dy^{3+}synthesized with Pechini and combustion methods.

Afterglow decay curves and fitted parameters are also shown in figure 4.15 and given table 4.8, respectively. According to the figure, 1% Co doped Pechini sample has the longest luminescence lifetime. Moreover, both Pechini samples have higher luminescence lifetime than combustion ones. We thought that this situation is directly related with crystalline structure of the sample. As mentioned before, the best luminescence properties can obtain only $SrAl_2O_4$ phase exist in the structure. According to XRD results, Pechini sample consist of only monoclinic $SrAl_2O_4$, so show higher luminescence properties.

Table 4.8 : Afterglow decay parameters of Co doped $SrA_{l2}O_4$: Eu^{2+}, Dy^{3+} phosphor synthesized with Pechini and combustion methods.

Samples	y_0	A_1	A_2	τ_1	τ_2
Comb. Co05	24,12	131,28	606,14	62,90	2,33
Comb. Co1	12,58	54,76	204,78	84,57	3,02
Pechini Co05	27,66	924,35	233,79	4,42	61,14
Pechini Co1	66,72	756,99	301,66	10,36	110,00

4.2.2 Effect of Fe

In order to investigate the effect of 0,5% and 1% Fe as dopant material on $SrAl_2O_4$:Eu^{2+}, Dy^{3+} phosphor, samples were synthesized with Pechini and combustion methods using raw materials in table 4.9.

Table 4.9 : Used raw materials for synthesizing of $Sr_{0,92-x}Fe_xAl2O4$:Eu^{2+}, Dy^{3+} (x=0,005 and 0,01)

Precursor materials	**Pechini**		**Combustion**	
	0.5% Fe	**1% Fe**	**0.5% Fe**	**1% Fe**
$Sr(NO_3)_2$	4,6473	4,6219	4,5842	4,5626
$Fe(NO_3)_3.9H_2O$	0,0484	0,0969	0,0478	0,0957
$Al(NO_3)_3.9H_2O$	18,0062	18,0062	17,7617	17,7751
Eu_2O_3	0,0844	0,0844	0,0833	0,0833
Dy_2O_3	0,2685	0,2685	0,2649	0,2651
H_3BO_3	0,1267	0,1267	5,2800	5,2760
$C_6H_8O_7.H_2O$	30,2601	30,2601		
CH_4N_2O	—		14,2281	14,2388

4.4.2.1 X-ray characterization

XRD patterns of 1% Fe-doped $SrAl_2O_4$:Eu^{2+}, Dy^{3+} synthesized with Pechini and combustion methods are given in figure 4.15. According to the figure, main phase is $SrAl_2O_4$ in both of XRD patterns. But combustion sample has an impurity phase in the structure. It can be seen from the figure that while doping of 1 % Fe in Pechini

method have almost no effect on crystalline structure, but causes the formation of an impurity phase in combustion case. Crystalline sizes of the samples are calculated according to 220 peak of $SrAl_2O_4$ and found as 17.11 and 34.24 nm for Pechini and combustion samples, respectively.

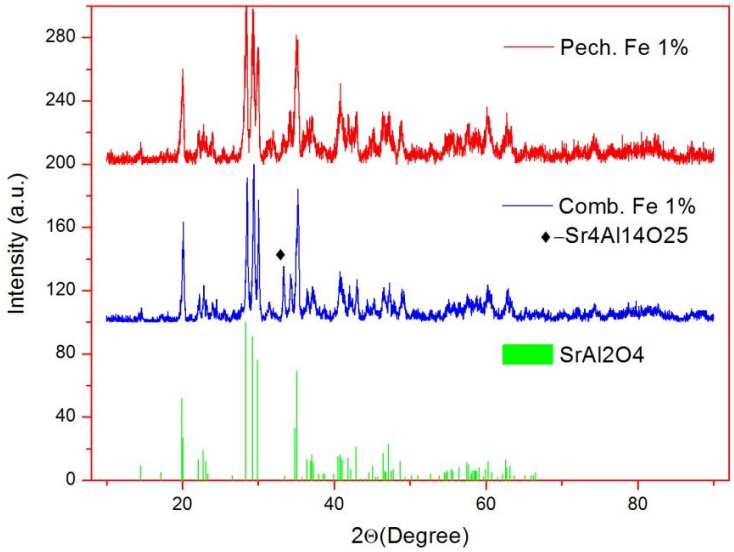

Figure 4.15 : XRD patterns of 1% Fe-doped $SrAl_2O_4:Eu^{2+}$, Dy^{3+} synthesized with Pechini and combustion methods.

4.4.2.2 Optical characterization

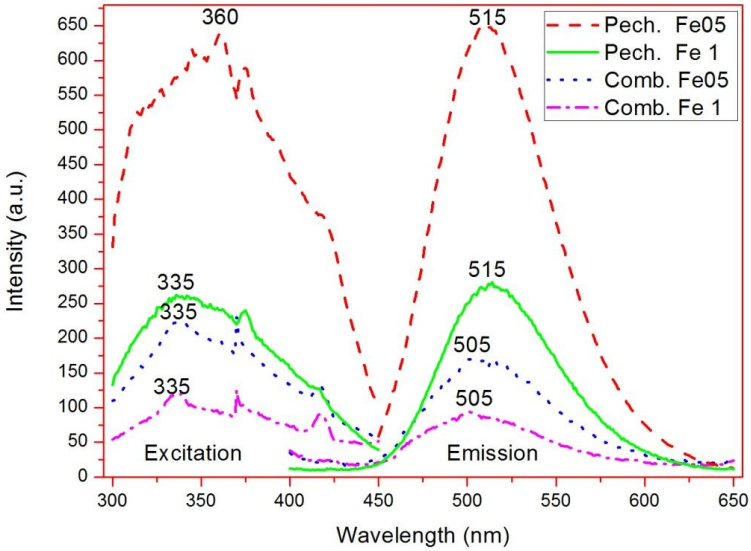

Figure 4.16 : Emission and excitation spectrums of Fe-doped $SrAl_2O_4:Eu^{2+}$, Dy^{3+} synthesized with Pechini and combustion methods.

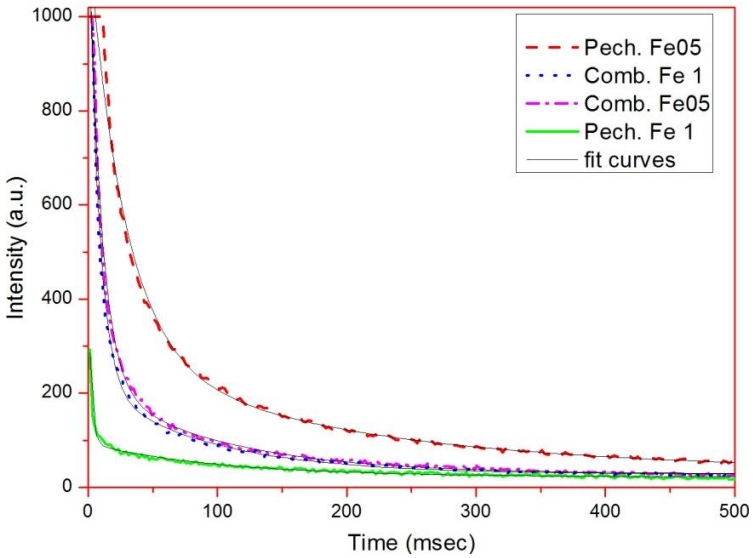

Figure 4.17 : Afterglow decay curves of Fe-doped $SrAl_2O_4:Eu^{2+}$, Dy^{3+}synthesized with Pechini and combustion methods.

In figure 4.16, emission and excitation spectrums of Fe-doped $SrAl_2O_4:Eu^{2+}$, Dy^{3+} synthesized with Pechini and combustion methods are given. According to the figure, Pechini sample with doping 0,5% Fe have maximum emission and excitation intensity peaked at 515 and 360 nm, respectively. When dopant concentration is 1% intensities of spectrums decrease. So, we can say that increasing doping concentration causes degreasing luminescence properties for Pechini case. Additionally, it is seen that Pechini samples have higher intensity in both spectrums than combustion samples.

In combustion case, when dopant concentration is 0.5%, samples have maximum emission and excitation intensity peaked at 505 and 335 nm, respectively. The same fact that increasing doping concentration causes degreasing luminescence properties is valid for combustion samples. Additionally, there are blue shifts in emission and excitation spectrums of both combustion samples.

When we look at afterglow curves of Fe doped Pechini and combustion samples, 0.5% Fe doped Pechini sample have the highest luminescence lifetime. Additionally, we can say that increasing doping concentration causes degreasing luminescence lifetime in both methods. This fact is more clear in Pechini samples than combustion ones. In table 4.10, afterglow parameters which are obtained by using equation 3.1 are given.

Table 4.10: Afterglow decay parameters of Fe-doped $SrAl_2O_4$: Eu^{2+}, Dy^{3+} phosphor synthesized with solid state, Pechini and combustion methods.

Samples	y_0	A_1	A_2	τ_1	τ_2
Comb. Fe05	28,39	196,11	962,91	98,02	9,98
Comb. Fe1	27,95	191,52	976,32	89,24	8,18
Pechini Fe05	35,43	876,79	250,62	28,01	186,75
Pechini Fe1	21,88	315,88	71,15	2,26	103,75

4.2.3 Effect of Ni

In order to investigate the effect of 0,5% and 1% Ni as dopant material on $SrAl_2O_4$:Eu^{2+}, Dy^{3+} phosphor, samples were synthesized with Pechini and combustion methods using raw materials in table 4.11.

Table 4.11: Used raw materials for synthesizing of $Sr_{0,92-x}Ni_xAl_2O_4$:Eu^{2+}, Dy^{3+} (x=0,005 and 0,01).

Precursor materials	Pechini		Combustion	
	0.5% Ni	1% Ni	0.5% Ni	1% Ni
$Sr(NO_3)_2$	4,5372	4,5124	4,5893	4,5642
$Ni(NO_3)_2 \cdot 6H_2O$	0,0340	0,0681	0,0344	0,0689
$Al(NO_3)_3.9H_2O$	17,5794	17,5794	17,7811	17,7811
Eu_2O_3	0,0824	0,0824	0,0834	0,0834
Dy_2O_3	0,2621	0,2621	0,2652	0,2652
H_3BO_3	0,1244	0,125	0,1249	0,1249
$C_6H_8O_7.H_2O$	29,5429	29,5429		
CH_4N_2O			14,2437	14,2437

4.2.3.1 X-ray characterization

XRD patterns of 1% Ni-doped $SrAl_2O_4$:Eu^{2+}, Dy^{3+} synthesized with Pechini and combustion methods are given in figure 4.18. Results are similar to Fe doped samples. Main phase is $SrAl_2O_4$ in both of XRD patterns and also an impurity phase ($Sr_4Al_{14}O_{25}$) with low peak intensity exists in the structure of Pechini and combustion samples. Calculated crystalline size using 220 peak of $SrAl_2O_4$ is 42.79nm for Pechini and 32.24nm for combustion samples.

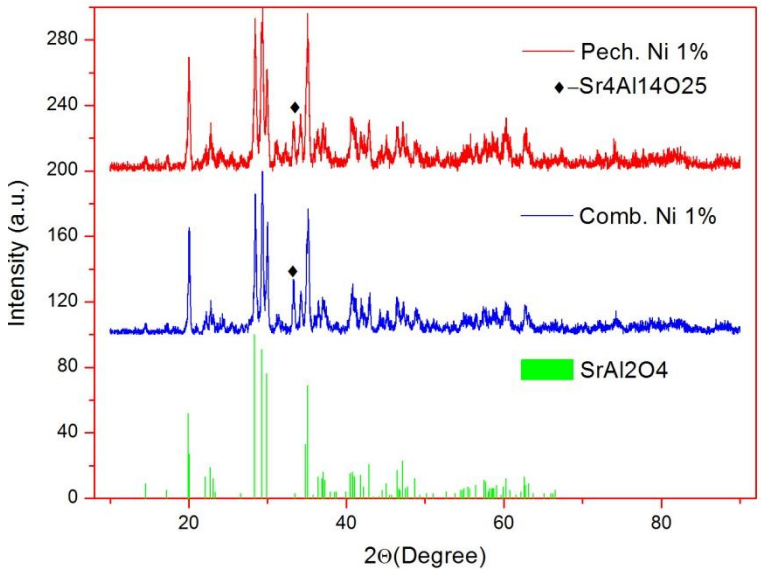

Figure 4.18 : XRD patterns of 1% Ni-doped $SrAl_2O_4$:Eu^{2+}, Dy^{3+} synthesized with Pechini and combustion methods

4.2.3.2 Optical characterization

All emission and excitation spectrums for all Ni-doped samples (figure 4.19) have nearly same shape and peaked at 515 and 333 nm, respectively. It is observed that intensity of spectrums is decreasing while dopant concentration of Ni is increasing for two methods. Additionally, combustion samples have relatively low luminescence properties. The same results are valid for afterglow decay curves (figure 4.20). Afterglow decay parameters of Ni-doped $SrAl_2O_4$: Eu^{2+}, Dy^{3+} phosphor synthesized with solid state, Pechini and combustion methods are given in table 4.12.

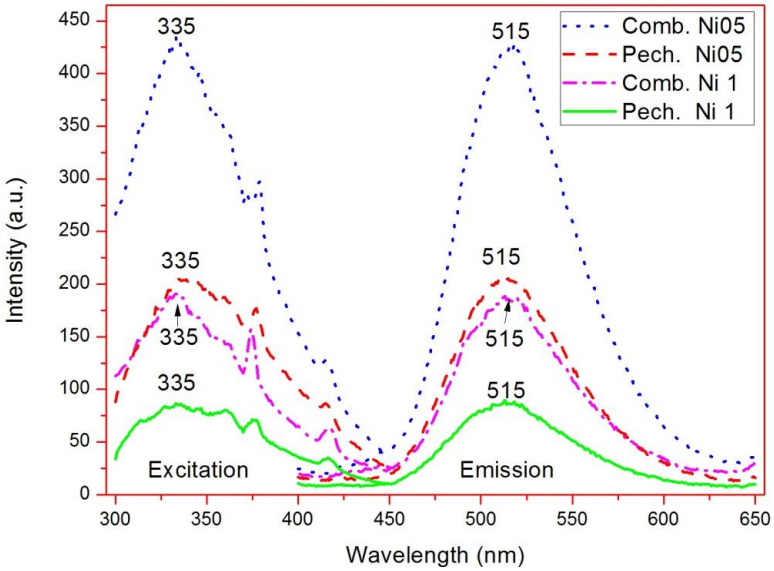

Figure 4.19 : Emission and excitation spectrums of Ni-doped $SrAl_2O_4$:Eu^{2+}, Dy^{3+} synthesized with Pechini and combustion methods

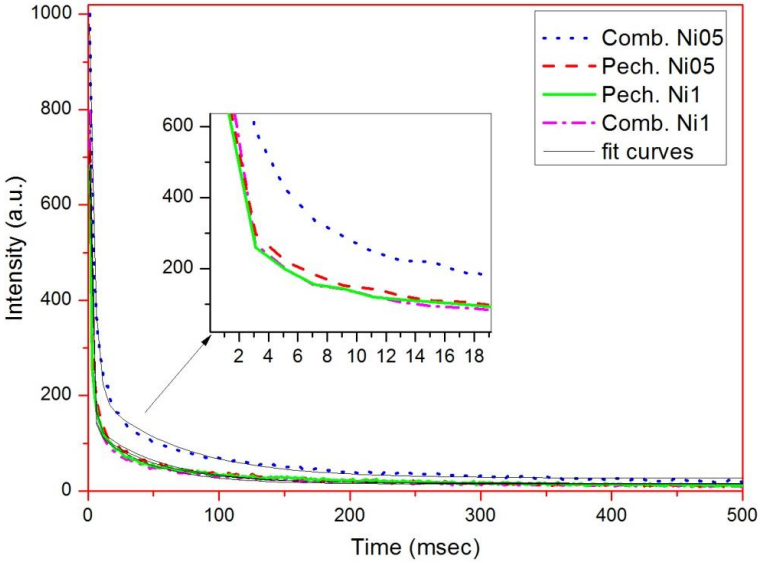

Figure 4.20 : Afterglow decay curves of Ni-doped $SrAl_2O_4:Eu^{2+}$, Dy^{3+}synthesized with Pechini and combustion methods.

Table 4.12 : Afterglow decay parameters of Ni-doped $SrAl_2O_4$: Eu^{2+}, Dy^{3+} phosphor synthesized with solid state, Pechini and combustion methods.

Samples	**y_0**	**A_1**	**A_2**	**τ_1**	**τ_2**
Comb. Ni05	27,02	1062,24	185,76	3,41	65,50
Comb. Ni1	14,56	1406,06	122,52	1,45	43,50
Pechini Ni05	15,65	1014,04	131,29	1,86	49,95
Pechini Ni1	16,41	1064,31	120,65	1,61	47,88

4.2.4 Effect of Y

In order to investigate the effect of 0,5% and 1% Y as dopant material on $SrAl_2O_4:Eu^{2+}$, Dy^{3+} phosphor, samples were synthesized with Pechini and combustion methods using raw materials in table 4.13.

Table 4.13 : Used raw materials for synthesizing of 5 g $Sr_{0,92-x}Y_xAl_2O_4:Eu^{2+}$, Dy^{3+} (x=0,005 and 0,01).

Precursor materials	**Pechini**		**Combustion**	
	0.5% Y	**1% Y**	**0.5% Y**	**1% Y**
$Sr(NO_3)_2$	4,5807	4,5555	4,5807	4,5555
$Y(NO_3)_3 \cdot 6H_2O$	0,0453	0,0906	0,0453	0,0906
$Al(NO_3)_3.9H_2O$	17,7478	17,7473	17,7478	17,7473
Eu_2O_3	0,0832	0,0832	0,0832	0,0832
Dy_2O_3	0,2647	0,2646	0,2647	0,2646
H_3BO_3	0,125	0,125	5,2841	0,125
$C_6H_8O_7.H_2O$	29,8259	29,8250		
CH_4N_2O			14,2170	14,2166

4.2.4.1 X-ray characterization

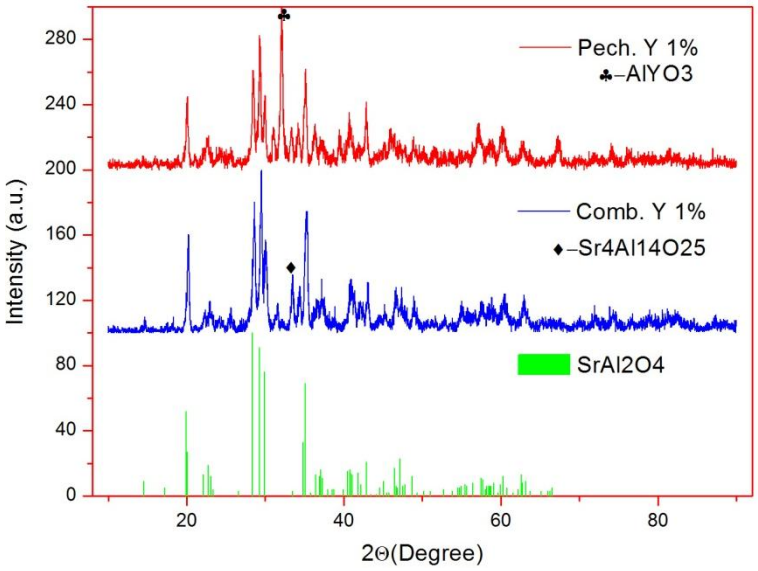

Figure 4.21 : XRD patterns of 1% Y-doped $SrAl_2O_4:Eu^{2+}$, Dy^{3+} synthesized with Pechini and combustion methods.

XRD patterns of 1% Y-doped $SrAl_2O_4:Eu^{2+}$, Dy^{3+} synthesized with Pechini and combustion methods are shown in figure 4.21. Main phase in the structure is $SrAl_2O_4$for both of the Pechini and combustion samples. While doping 1% Y did not cause the formation of any Y_2O_3- Al_2O_3 compound in combustion sample, there is an Y_2O_3- Al_2O_3 compound ($AlY0_3$) in Pechini sample. Calculated crystalline size using 220 peak of $SrAl_2O_4$is 28.53 nm for Pechini and 34.25 nm for combustion samples.

4.2.4.2 Optical characterization

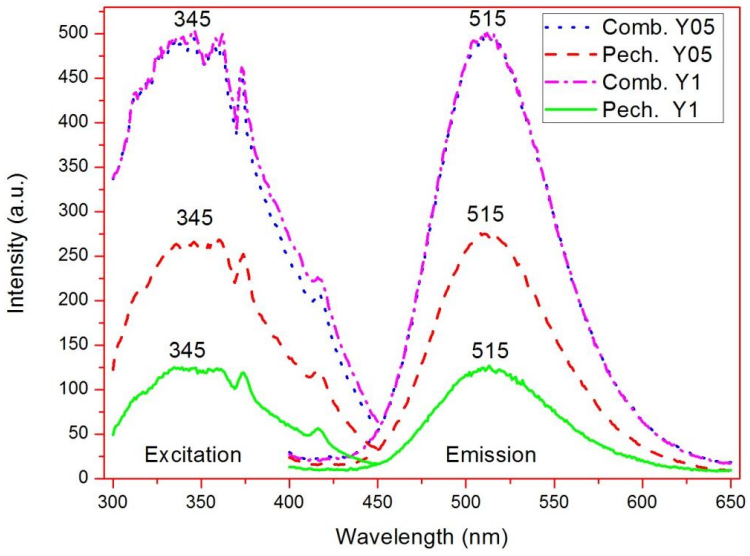

Figure 4.22 : Emission and excitation spectrums of Y-doped $SrAl_2O_4:Eu^{2+}$, Dy^{3+} synthesized with Pechini and combustion methods.

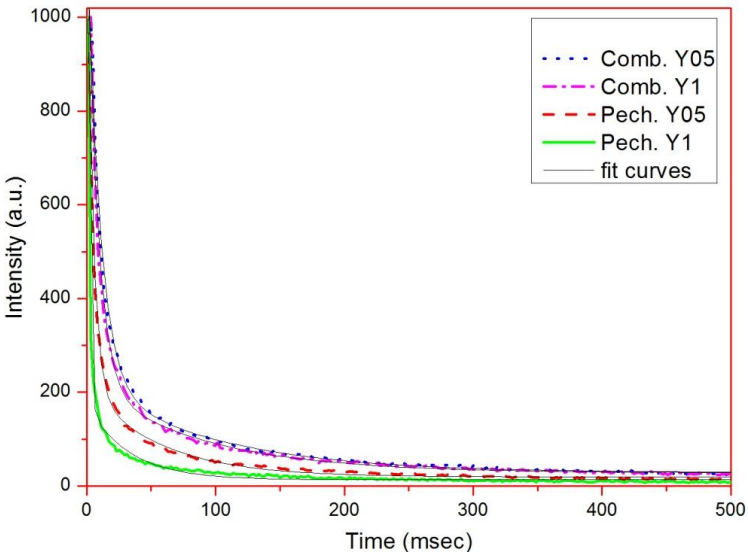

Figure 4.23 : Afterglow decay curves of Y-doped $SrAl_2O_4:Eu^{2+}$, Dy^{3+}synthesized with Pechini and combustion methods.

Emission and excitation spectrums of Y-doped $SrAl_2O_4:Eu^{2+}$, Dy^{3+} synthesized with Pechini and combustion methods are shown in figure 4.22. According to the figure, Y-doped samples synthesized with two methods have nearly the same shape of emission and excitation spectrums peaked at 515 and 345 nm, respectively. We can say that concentration of doped Y has no effects on combustion samples. But, the case is different in Pechini samples. 0,5 % Y-doped Pechini sample has higher intensities in both of spectrum than 1 % Y-doped one. The same results can be seen in afterglow decay time curves (figure 4.23). In table 4.14, afterglow decay parameters are shown. Samples can be sort from long to short in terms of decay time as comb. Y05, comb.Y1, Pechini Y05 and Pechini Y1. It can be said that increasing concentration causes to decreasing in luminescence lifetime in both of two methods.

Table 4.14 : Afterglow decay parameters of Y-doped $SrAl_2O_4$: Eu^{2+}, Dy^{3+} phosphor synthesized with solid state, Pechini and combustion methods.

Samples	**y_0**	**A_1**	**A_2**	**τ_1**	**τ_2**
Comb. Y05	28,39	196,11	962,91	98,02	9,98
Comb. Y1	27,95	191,52	976,32	89,24	8,18
Pechini Y05	19,28	996,30	193,02	4,51	55,99
Pechini Y1	13,09	1906,44	158,57	1,324	33,42

5. CONCLUSION

Synthesis of some transition metals and Y doped $SrAl_2O_4$ based nanophosphor particles is one of the aims of this thesis. In this section we compare and conclude the results of optical analysis of doped combustion and Pechini samples.

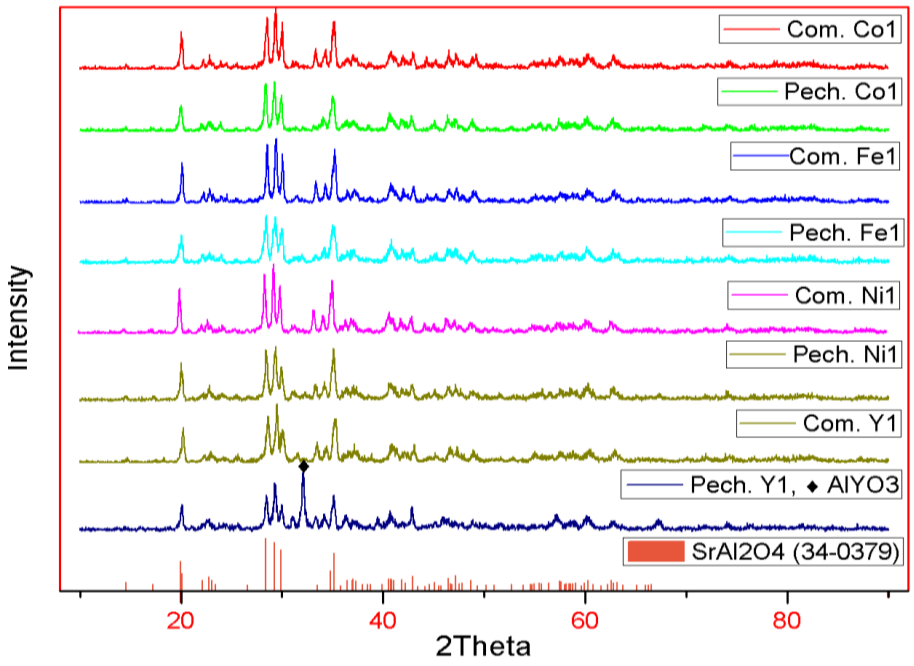

Figure 5.1 : XRD patterns of 1% Co, Fe, Ni and Y doped Pechini and combustion samples.

XRD patterns of all doped Pechini and combustion samples are given in figure 5.1. According to figure, monoclinic $SrAl_2O_4$ is the main phase for all doped samples. Additionally, we can see an impurity phase ($AlYO_3$) with very high peak intensity in the 1% yttrium doped Pechini sample. Crystalline sizes of the samples were calculated using Scherrer formula according to 220 peak of the $SrAl_2O_4$and found in 17-42 nm range. In table 5.1, calculated grain sizes of the samples are given.

Table 5.1 : Calculated crystallite size for doped samples.

Samples	**Pechini 1% doped**				**Combustion 1% doped**			
Dopant	Co	Fe	Ni	Y	Co	Fe	Ni	Y
Crystalline size (nm)	28,52	17,11	42,79	28,53	34,24	34,24	34,24	34,25

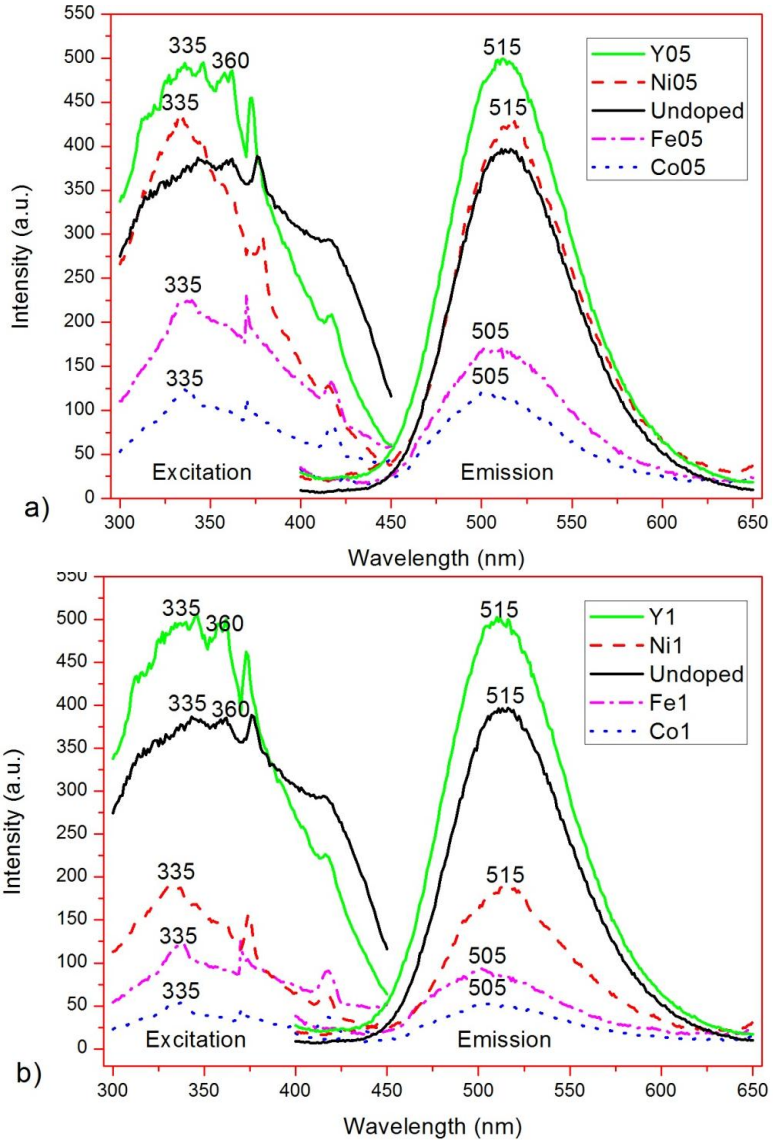

Figure 5.2 : Emission and excitation spectrums of $Sr_{0,92-X}M_XAl_2O_4$: Eu^{2+}, Dy^{3+} (M=Co, Fe, Ni, Y) a) X= 0,005 and b) X=0,01 phosphors synthesized with combustion method annealed in H_2/N_2 RA for 1 h.

In figure 5.2-a, emission and excitation spectrums of $Sr_{0,915}M_{0,005}Al_2O_4$: Eu^{2+}, Dy^{3+} (M=Co, Fe, Ni, Y) phosphors synthesized with combustion method annealed in H_2/N_2 reducing atmosphere for 1 hour. In general, the peaks at 505 – 515 nm emission spectrums belongs to $4f^65d^1 \rightarrow 4f^7$ electronic transition of Eu^{2+} ions which are assumed to occupy Sr(II) sites in the structure. To compare the optical performances of doped samples, un-doped $SrAl_2O_4$:Eu^{2+}, Dy^{3+} combustion sample is selected as reference sample. While 0,5% doped Y and Ni affect the emission spectrums (peaked at 515 nm) in positive way, 0.5% doped Co and Fe reduced the emission intensity quietly and cause a blue shift in emission peaks (peaked at 505

nm). The same effect can be seen in excitation line. We also see a narrowing in excitation spectrums for all doped samples.

When dopant concentration increases to 1%, we see decreasing in intensity of emission and excitation spectrums of Fe, Ni and Co doped sample. However, increasing in concentration of Y has almost no effect on luminescence properties.

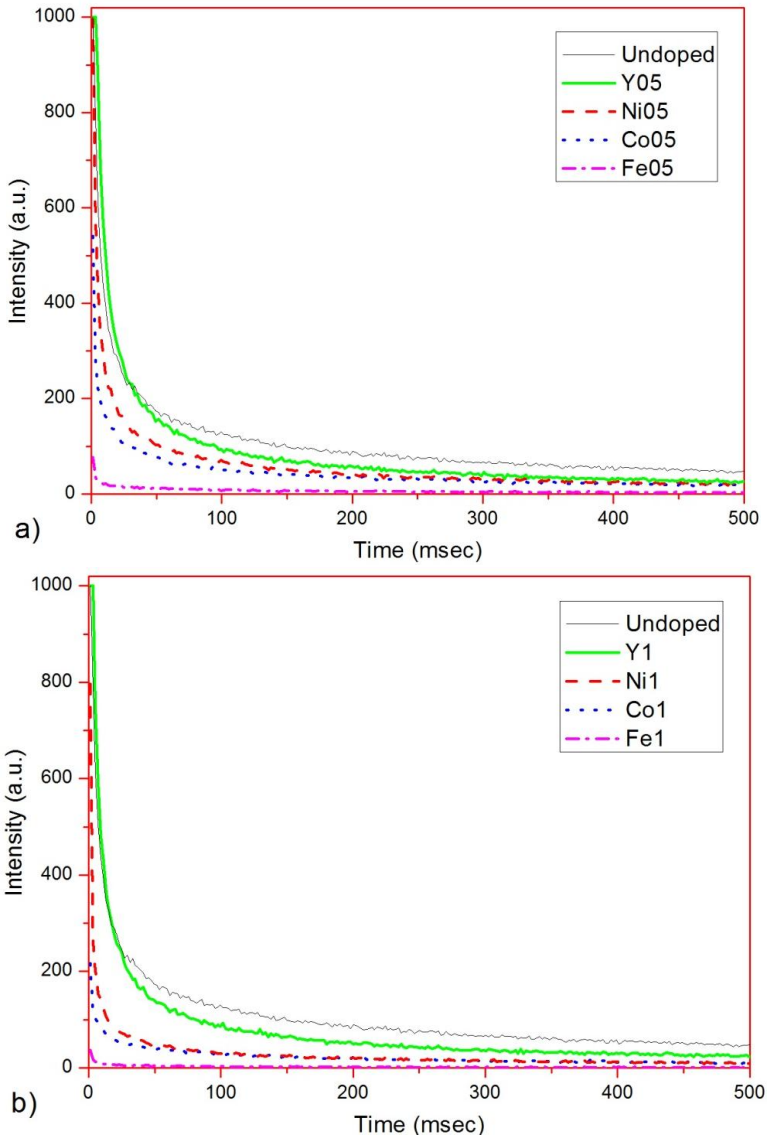

Figure 5.3 : Emission and excitation spectrums of $Sr_{0,92-X}M_XAl_2O_4$: Eu^{2+}, Dy^{3+} (M=Co, Fe, Ni, Y) a) X= 0,005 and b) X=0,01 phosphors synthesized with combustion method annealed in H_2/N_2 RA for 1 h.

When we look afterglow decay curves (figure 5.3-a and b), luminescence lifetimes for all doped samples have decreased compared with un-doped one. Additionally, increasing concentration of these dopant ions has negative effect on luminescence lifetime of phosphors. But Y doped samples has no deducible effect on luminescence

lifetime like emission/ excitation spectrum even dopant concentration is 1%. In table 5.1, afterglow decay parameters of all combustion samples can be seen.

Table 5.2 : Afterglow decay parameters of $Sr_{0,915}M_{0,005}Al_2O_4$: Eu^{2+}, Dy^{3+} (M=Co, Fe, Ni, Y) combustion samples.

Comb. Samples		**y_0**	**A_1**	**A_2**	**τ_1**	**τ_2**
Un-doped		131,17	402,19	558,78	164,49	19,25
0,5 %	Y	28,39	196,11	962,91	98,02	9,98
	Ni	27,02	1062,24	185,76	3,41	65,50
	Co	24,12	131,28	606,14	62,90	2,33
	Fe	28,39	196,11	962,91	98,02	9,98
1 %	Y	27,95	191,52	976,32	89,24	8,18
	Ni	14,56	1406,06	122,52	1,45	43,50
	Co	12,58	54,76	204,78	84,57	3,02
	Fe	27,95	191,52	976,32	89,24	8,18

The effect of dopant types and concentration on luminescence properties of Pechini samples is shown in figure 5.4 and 5.5. We can see emission pattern of Eu^{2+} due to $4f^65d^1 \rightarrow 4f^7$ electronic transitions for all samples. In Pechini method, except Fe all 0,5% doped samples shows lower emission and excitation performance than reference sample. Moreover, increasing in dopant concentration affects the performance negatively for all samples. Although Y has positive effect on performance of combustion samples, the same effect is not valid for Pechini ones. This situation may be due to the possibility of obtaining non-homogeneous precursor gel in Pechini method. Additionally, concentration of dopant ions has different effects on performance from combustion, too. In combustion, optical performances of samples decrease while dopant concentration of ions (except Y) is increasing; we cannot generalize this effect in Pechini samples. For example, in cobalt case, increasing concentration of cobalt ions causes increasing optical performance in Pechini.

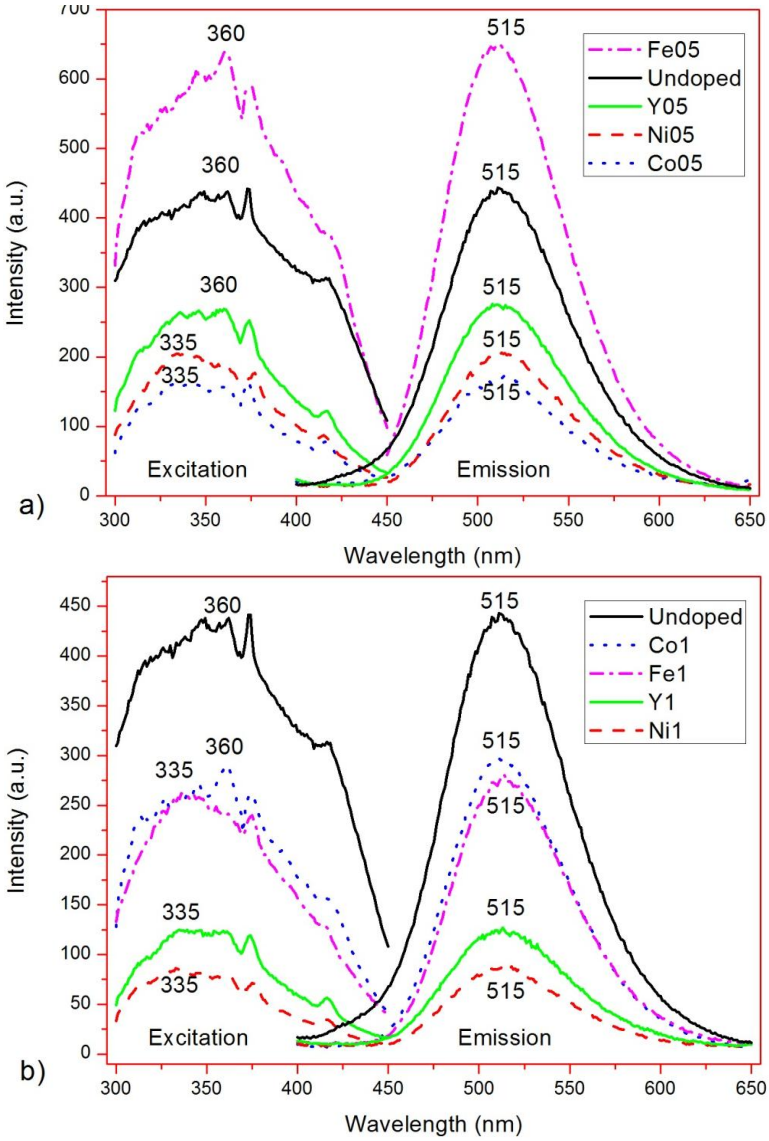

Figure 5.4 : Emission and excitation spectrums of $Sr_{0,92-X}M_XAl_2O_4$: Eu^{2+}, Dy^{3+} (M=Co, Fe, Ni, Y) a) X= 0,005 and b) X=0,01 phosphors synthesized with Pechini method annealed in H_2/N_2 RA for 1 h.

In afterglow decay curve (figure 5.5-a and b) all doped samples without depending on amount of concentration, show worse lifetime than un-doped one. Except Co doped sample, increasing dopant concentrations causes decreasing in lifetime. In table 5.3, afterglow parameters all Pechini samples are given.

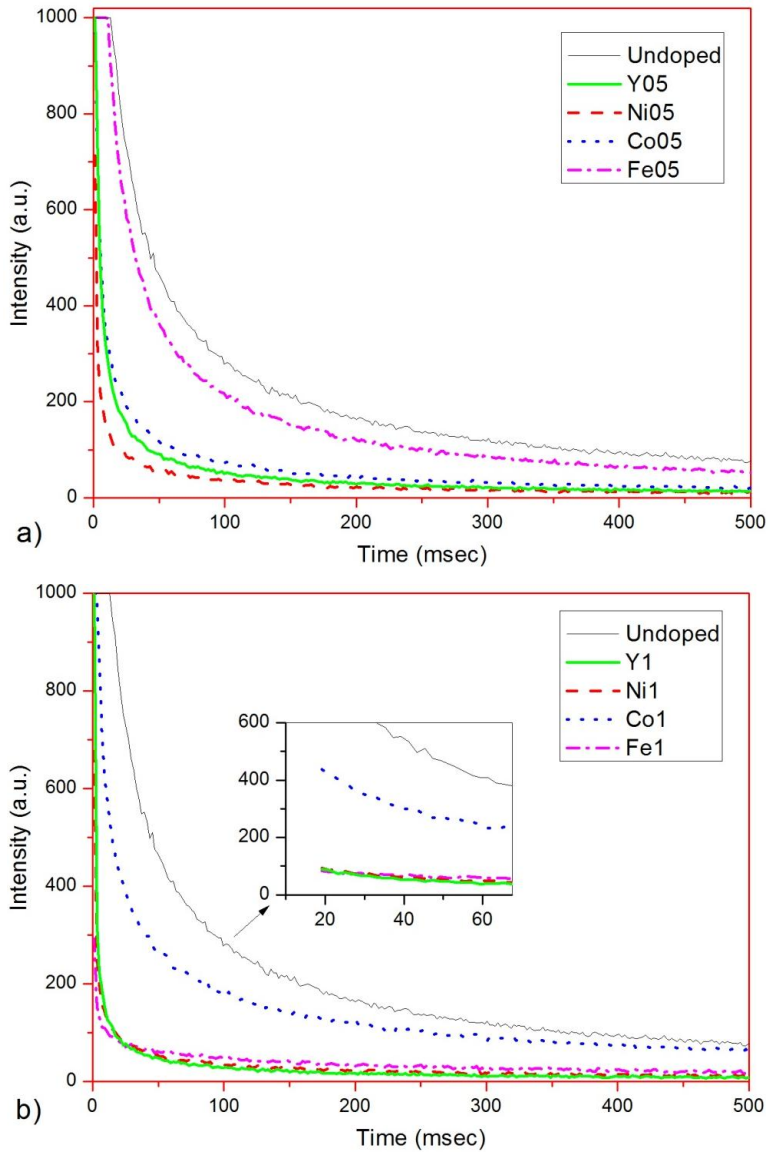

Figure 5.5 : Emission and excitation spectrums of $Sr_{0,92-X}M_XAl_2O_4$: Eu^{2+}, Dy^{3+} (M=Co, Fe, Ni, Y) a) X= 0,005 and b) X=0,01 phosphors synthesized with combustion method annealed in H_2/N_2 RA for 1 h.

Table 5.3 : Afterglow decay parameters of $Sr_{0,915}M_{0,005}Al_2O_4$: Eu^{2+}, Dy^{3+} (M=Co, Fe, Ni, Y) Pechini samples.

Pechini Samples		**y_0**	**A_1**	**A_2**	**τ_1**	**τ_2**
Un-doped		31,51	265,57	851,81	275,00	38,54
0,5 %	Y	19,28	996,30	193,02	4,51	55,99
	Ni	15,65	1014,04	131,29	1,86	49,95
	Co	27,66	924,35	233,79	4,42	61,14
	Fe	35,43	876,79	250,62	28,01	186,75
1 %	Y	13,09	1906,44	158,57	1,32	33,42
	Ni	16,41	1064,31	120,65	1,61	47,88
	Co	66,72	756,99	301,66	10,36	110,00
	Fe	21,88	315,88	71,15	2,26	103,75

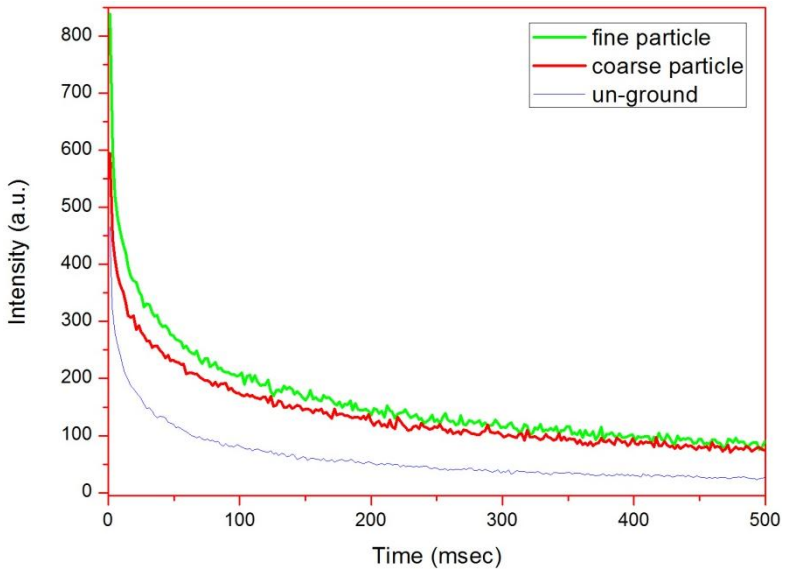

Figure 5.6 : Effect of particle size on luminescence lifetime.

In figure 5.6, afterglow decay curves of the un-doped Pechini sample with different particle size are given. According to the figure, luminescence lifetime increases while particle size is getting smaller. This result can be attributed to higher surface area of the smaller particles. So, when particle size is smaller, the sample absorbs more incident light which results more excitation and longer lifetime.

6. GENERAL CONCLUSIONS

In this experimental study, synthesizing of nano crystalline sized $SrAl_2O_4$ based phosphors is achieved in three different fabrication methods (solid state, Pechini and combustion). Additionally, according to $Sr_{0,92-X}M_XAl_2O_4:Eu_{0,02},Dy_{0,06}$(M=Co, Ni, Fe, Y) chemical formula, totally 16 samples were synthesized and characterized to investigate the effect of some transition metals and yttrium on optical performance of this phosphor. Obtained all data from experimental studies are given two main headings: First, the effect of synthesizing methods and the second, the effect of dopant on structural and optical performances.

To optimize the effective reaction time in 5% H_2/N_2 reduced atmosphere, three samples in the same composition were prepared and sintered at 1300°C for 1, 3 and 6 hours. According to XRD results, although there are two impurity phases in the structure, monoclinic $SrAl_2O_4$ is the main phase for all samples. Additionally, peak intensity of the $SrAl_2O_4$ is increasing with the increasing of reaction time. Spectrophotometric analyses were carried out to these samples and it is observed that intensities of emission and excitation spectrums and also afterglow decay lifetime are increasing with the increasing of reaction time.

The methods used in the synthesis of phosphor materials influence the structural properties of the products in different ways. While only monoclinic $SrAl_2O_4$ phase with nearly same peak intensity was observed in XRD patterns of Pechini and combustion samples, monoclinic $SrAl_2O_4$with weaker peak intensity and additional impurity phases were observed in XRD pattern of the solid state sample.

Spectrophotometric analysis showed that all samples have emission and excitation with different intensities. Additionally, emission spectrums have the same shape and peaked at 515 nm for all samples; excitation spectrums are different in shape and peaked at different wavelength. Since different synthesizing methods form different lattice defects in the structure which changes crystal field near the Eu^{2+} ions, excitation spectrums have different shape. Besides, these emission spectrums have same shape due to emission center ($4f^6 \rightarrow 5d^1$electronic transition of Eu(II)) is the

same in the all structures. Combustion sample has the highest luminescence intensity and luminescence decay lifetime and it followed by Pechini and solid state samples, respectively.

Trapping - detrapping is recommended mechanism for persistent phosphorescence of this type phosphors. According to this mechanism, excited electrons of Eu^{2+} ions captured by the trap levels and then these electrons slowly released when they have enough thermal energy. Initial fast and then slow decay rate is a result of this mechanism. It is observed from lifetime measurement that all samples show this type of phosphorescence characteristics.

Dopant materials affected the optical properties of the samples differently depending on their fabrication methods. So, we thought that inconsistency in the literature for same composition is due to using different fabrication methods. In our study, for combustion case, we obtained improvement in the intensities of emission and excitation spectrums of the $SrAl_2O_4:Eu^{2+},Dy^{3+}$ phosphor with addition of only 0.5%Y and Ni as co-dopant. Additionally, increasing co-dopant concentration causes decreasing intensities of these spectrums in all dopants except Y. Increasing Y content up to 1% is almost no effect on the spectrum intensity. Therefore, Ni, Fe and Co co-doped samples have same shape excitation spectrums peaked at the same point and also, doping of Co and Fe causes a blue shift in emission peaks (peaked at 505 nm).

In Pechini case, all samples have same shape emission spectrums peaked at 515 nm with different intensities. Only 0,5% co-doped Fe sample improve the emission and excitation intensities. Increasing dopant concentration causes decreasing intensities and luminescence lifetime of the $SrAl_2O_4$ based phosphor for all doping cases except Co. Increasing Co concentration up to 1% increase the optical performance.

REFERENCE

[1] Ozawa, L., 2007, Cathodoluminescence and Photoluminescence Theories and Practical Applications, CRC Press.

[2] Ye, S., Xiao, F., Pan, Y.X., Ma, Y. Y., Zhang, Q.Y., 2010, Phosphors In Phosphor-Converted White Light-Emitting Diodes: Recent Advances In Materials, Techniques and Properties, Vol: 71, Issue: 1, pp: 1–34.

[3] Yen, W. M., Shionoya, S., Yamamoto, H., 2007, Second Edition Phosphor Handbook, CRC Press.

[4] Matsuzawa, T., Aoki, Y., Takeuchi, N. and Murayama, Y., 1996, A New Long Phosphorescent Phosphor with High Brightness $SrAl_2O_4:Eu^{2+,}$ D^{3+}, J. Electrochemical Society, Vol: 143, No.8.

[5] Song, H. and Chen,D., 2007, Combustion synthesis and luminescence propertiesof $SrAl_2O_4:Eu^{2+}$, Dy^{3+}, Tb^{3+} phosphor, Luminescence, Vol: 22, pp. 554 558.

[6] Yoshihiko M., Nobuyoshi, T., Yasumitsu, A., Takashi, M., 1994, Phosphorescent Phosphor, European Patent Office, No: 0622440A1 dated 01.11.04.

[**7] Uluç, A. V.,** 2008, Synthesis and Characterization of Phosphorescent Strontium Aluminate Compounds, M.Sc Thesis, Sabancı University, Istanbul

[8] Faridnia, B. and Motlagh, M.K.,2007, Optimizing Synthesis Conditions for Long Lasting $SrAl_2O_4$ Phosphor, Pigment & Resin Tech. Vol: 36, No: 4, pp. 216–223.

[9] Ayvacıklı, M., Khatab, A., Ege, A., Şabikoğlu, İ., Henini, M. and Can N., 2012, Absorption and Photoluminescence Spectroscopy of Er3+-doped $SrAl_2O_4$ Ceramic Phosphors, Philosophical Magazine Letters, Vol: 92, No:4, pp.194-201.

[10] Song, H., Chen, D., Tang, W. and Peng, Y., 2008, Synthesis of $SrAl_2O_4:Eu^{2+}$, Dy^{3+}, Gd^{3+} Phosphor by Combustion Method and Its Phosphorescence Properties, Displays, 29, pp. 41–44

[11] G. G. Stokes, 1852, On the Change of Refrangibility of Light, Phil. Trans. R. Soc. Lond. Vol: 142, pp. 463-562.

[12] Url-1 <http://physik.unibas.ch/Praktikum/VPII/Fluoreszenz/Fluorescence_and_Phosphorescence.pdf>, Citation date 06.04.2014.

[13]Url-2 <http://einstein.sc.mahidol.ac.th/~jose/pdf/photoluminescence.pdf>, Citation date 09.03.2014.

[14] Albani, J. R., 2007, Principles and Applications of Fluorescence Spectroscopy, Blackwell Publishing.

[15] Valeur, B. and Brochon, J. C., 2001, New Trends in Fluorescence Spectroscopy, Springer.

[16] Vij, D.R. and Singh, N., 1998, Luminescence and Related Properties of II-VI Semiconductors, Nova Science Publishers.

[17] Url-3 <http://www.tf.uni-kiel.de/matwis/amat/admat_en/kap_5/advanced/t5_2_4.html>, Citation date 20.03.2014

[18] Url-4 <http://uvminerals.org/fms/luminescence>, Citation date 01.04.2014.

[**19] William, M. Yen, Shigeo Shionoya, Hajime Yamamoto,** 2007, Practical Applications of Phosphors, CRC Press.

[20] Peng, T. andYang,H., 2003, Combustion Synthesis and Photoluminescence of $SrAl_2O_4$: Eu, DyPhosphor Nanoparticles, Materials Letters Vol. 58 pp. 352-356

[21]Van den Eeckhout, K., Smet, P. F. and Poelman, D., 2010, PersistentLuminescence in Eu^{2+}-Doped Compounds: A Review, Materials Vol.3, pp.2536-2566.

[22] Douy, A., and Capron, M. , 2003, Crystallization of Spray-dried Amorphous Precursors in the $SrO\text{-}Al_2O_3$ system: a DSC Study, Journal of the European Ceramic Society, Vol: 23, No: 12, pp. 2075-2081.

[23] Ryu, H., Bartwal, K.S., 2009, Defect structure and its relevance to photoluminescence in $SrAl_2O_4$:Eu^{2+}, Nd^{3+}, Physica B, 404, 1714-1718.

[24] Lü, X., Shu, W., Yu, Q., Fang, Q., 2007,Roles Of Doping Ions In Persistent Luminescence of $SrAl_2O_4$: Eu^{2+}, RE^{3+} Phosphors, Glass Physics and Chemistry, Vol. 33, no. 1, pp. 62–67

[25]Url-3 <http://www.periodni.com/slike/monoclinic.gif>, Citation date 09.04.2014.

[26]Peng, T., Huajun, L., Yang H. and Yan, C., 2003, Synthesis of $SrAl_2O_4$: Eu, Dy Phosphor Nanometer Powders by Sol–Gel Processes and Its Optical Properties, Materials Chemistry and Physics 85 pp. 68–72

[27] Aitasalo, T., Deren, P.,Holsa, J.,Jungner, H. and Krupa, J.-C., 2002, Persistent luminescence phenomena in materials doped with rare earth ions, Journal of Solid State Chemistry 171 114–122

[28] P. Dorenbos, 2005, Mechanism of Persistent Luminescence in $Eu^{2+}$and Dy^{3+}, Journal of the Electrochemical Society, 152 (7) H107-H110

[29] P. Dorenbos, 2004, Locating lanthanide impurity levels in the forbiddenband of host crystals,Journal of Luminescence 108 301–305

[30] P. Dorenbos, 2004, Mechanism of persistent luminescence in $Sr_2MgSi_2O_7$:Eu^{2+}, Dy^{3+}, phys. stat. sol. (b) 242, No. 1

[31] Clabau, F., Rocquefelte, X. and Jobic, S., 2005, Mechanism of Phosphorescence Appropriate for the Long-Lasting Phosphors Eu^{2+}-doped $SrAl_2O_4$ with Co-dopants Dy^{3+} and B^{3+}, Chem. Mater. 17 (15), pp 3904–3912

[32] Clabau, F., Rocquefelte, X.,Jobic, S. and Deniard, P., 2007, On the phosphorescence mechanism in SrAl2O4:Eu2+and its co-doped derivatives, Solid State Sciences 9 608-612

[33] Aitasalo, T.,Hölsä, J.,Jungner, H., Lastusaari, M. and Niittykoski, J., 2006, Thermoluminescence Study of Persistent Luminescence Materials: Eu^{2+}- and R^{3+}-doped calcium aluminates, $CaAl_2O_4:Eu^{2+}$, R^{3+}, J Phys. Chem. B.110(10):4589-98.

[34] Han, S., Singh, K., Cho, T., Lee, H., Kim J., Chun I., Gwak J., 2008, Preparation and Characterization of Long Persistence Strontium Aluminate Phosphor, Journal of Luminescence, Vol: 128, No: 3, pp. 301-305

[35] Chang Y., Hsiang H., Liang, M., 2008, Characterization of Eu, DyCo-Doped $Sral_2o_4$ Phosphors Prepared by the Solid-State Reaction with B_2O_3Addition, Journal of Alloys and Compounds, Vol: 461, pp. 598-603.

[36] Xiao, L., Xiao, Q., and Liu, **Y.,** 2010, Preparation and characterization of flower-like SrAl2O4:Eu2+, Dy3+ phosphors by sol-gel process, Journal of Rare Earths, Vol. 29, No. 1, p. 39

[37] Patil, K. C., Aruna, S.T. and Ekambaram,m S., 1997, Combustion Synthesis.Current Opinion in Solid State & Materials Science, 2:1568-165

[38] McKittrick, J., Shea, L.E., Bacalski, C.F. and Bosze, E.J. 1999, The influence of processing parameters on luminescent oxides produced by combustion synthesis, Displays 19, 169–172

[39] Kingsley, J.J. and Pederson, L.R., 1993, Energetic materials in ceramics synthesis, Mat. Res. Soc. Symp. Proc. 296 361–366

[40] Yu X., Zhou C., He X., Peng Z., Yang S., 2004, The influence of some processing conditions on luminescence of $SrAl_2O_4:^{Eu2+}$ nanoparticles produced by combustion method, Materials Letters 58 1087 – 1091

[41] Höppe, H. A., 2009, Recent Developments in the Field of Inorganic Phosphors, Angew. Chem. Int. Ed., 48[357] 2–82.

[42] H. Yamamoto, 2010, White LED Phosphors: The Next Step Proc. SPIE, 7598, 759808-1.

[43] Pengpeng D., Xintong Z., Panpan S., Jikai Y., Shili Y., and Yichun L., 2012, Influence of Flux on Morphology and Luminescence Properties of Phosphors: A Case Study on $Y_{1.55}Ti_2O_7$:0.45Eu^{3+}, J. Am. Ceram. Soc., 95:1447–1453.

[44] Nag A., Kutty T. R. N., 2003, Role of B_2O_3 on the phase stability and long phosphorescence of $SrAl_2O_4$: Eu, Dy, Journal of Alloys and Compounds, Vol: 354, No: 1-2, pp. 221-231.

[45] Tang, ZL; Zhang, F; Zhang, Z. T., 2000, Luminescent properties of $SrAl_2O_4$:Eu, Dy material prepared by the gel method. Journal of the European Ceramic Society 20 2129-2132

CURRICULUM VITAE

Name, Surname	: **Mehmet Durmuş ÇALIŞIR**
Date and Place of Birth	: **Kars**, **1988**
E-mail	: **mehmetdcalisir@gmail.com**

EDUCATION:

B.Sc.	**:** Gebze Institute of Technology, Materials Science and Engineering, 2012; Electronics Engineering, 2012.
M.Sc.	**:** Istanbul Technical University, Nano-Science and Nano-Engineering, 2014